Artificial Neural Networks for Location Estimation and Co-Channel Interference Suppression in Cellular Networks

By

Javed Muhammad

A Thesis submitted to the

University of Stirling

in partial fulfilment of the requirements for the degree of

Master of Philosophy

Department of Computing Science and Mathematics

February 2007

Declaration

I declare that the thesis has been composed by myself and that it embodies the results of my own research. Where appropriate, I have acknowledged the nature and extent of work carried out in collaboration with others included in the thesis.

Acknowledgements

I am grateful to my Supervisor, Dr. Amir Hussain for his excellent guidance and support, which resulted in the completion of this Thesis.

Secondly, I would like to thank my former employer (Solectron UK) who provided the funding for this degree. Aside from acknowledging the many friends that have made my time at Stirling pleasurable, I would especially like to thank Dr. Nhamo Mtetwa, Dr. Ali Zayed, for the many fruitful discussions relating to this thesis.

Finally, I would like to thank all of my friends and family for their continued support and encouragement.

Abstract

This thesis reports on the application of artificial neural networks to two important problems encountered in cellular communications, namely, location estimation and co-channel interference suppression. The prediction of a mobile location using propagation path loss (signal strength) is a very difficult and complex task. Several techniques have been proposed recently mostly based on linearized, geometrical and maximum likelihood methods. An alternative approach based on artificial neural networks is proposed in this thesis which offers the advantages of increased flexibility to adapt to different environments and high speed parallel processing. Location estimation provides users of cellular telephones with information about their location. Some of the existing location estimation techniques such as those used in GPS satellite navigation systems require non-standard features, either from the cellular phone or the cellular network. However, it is possible to use the existing GSM technology for location estimation by taking advantage of the signals transmitted between the phone and the network. This thesis proposes the application of neural networks to predict the location coordinates from signal strength data. New multi-layered perceptron and radial basis function based neural networks are employed for the prediction of mobile locations using signal strength measurements in a simulated COST-231 metropolitan environment. In addition, initial preliminary results using limited available real signal-strength measurements in a metropolitan environment are also reported comparing the performance of the neural predictors with a conventional linear technique. The results

indicate that the neural predictors can be trained to provide a near perfect mapping using signal strength measurements from two or more base stations.

The second application of neural networks addressed in this thesis, is concerned with adaptive equalization, which is known to be an important technique for combating distortion and Inter-Symbol Interference (ISI) in digital communication channels. However, many communication systems are also impaired by what is known as co-channel interference (CCI). Many digital communications systems such as digital cellular radio (DCR) and dual polarized micro-wave radio, for example, employ frequency re-usage and often exhibit performance limitation due to co-channel interference. The degradation in performance due to CCI is more severe than due to ISI. Therefore, simple and effective interference suppression techniques are required to mitigate the interference for a high-quality signal reception. The current work briefly reviews the application of neural network based non-linear adaptive equalizers to the problem of combating co-channel interference, without a priori knowledge of the channel or co-channel orders. A realistic co-channel system is used as a case study to demonstrate the superior equalization capability of the functional-link neural network based Decision Feedback Equalizer (DFE) compared to other conventional linear and neural network based non-linear adaptive equalizers.

Table of contents

List of Figures

List of Abbreviations

A-GPS	Assisted-GPS
ANN	Artificial Neural Network
AOA	Angle of Arrival
AWGN	Additive White Gaussian Noise
BER	Bit Error Rate
BPNN	Back Propagation Neural Network
BPSK	Binary Phase Shift Keying
BS	Base Station
BTS	Base Transceiver Station
CCI	Co-Channel Interference
CCIR	Comité Consultatif International des Radio-Communication
CDMA	Code Division Multiple Access
COST	Cooperation in the field of Scientific and Technical Research
CS	Control Centre
dBW	Decibel Watts
DCR	Digital Cellular Radio
DCS	Digital Cellular System
DDM	Decision Direct Mode
DECT	Digital Enhanced Cordless Telecommunications
DFE	Decision Feedback Equalizer
DFFLE	Decision Feedback Functional Link Equalizer
DFWNE	Decision Feedback Wave Net Equalizer
DR	Delta Rule
E-OTD	Enhanced Observed Time Difference
FDTD	Finite-Difference Time-Domain
FIR	Finite Impulse Response
GHz	Giga Hertz
GPRS	General Packet Radio Service
GPS	Global Positioning System
GRNN	Generalized Regression Neural Network
GSM	Global System for Mobile Communications
GTD	Geometrical Theory of Diffraction
HLR	Home Location Register
HOS	Higher Order Statistics
ISI	Inter-Symbol Interference
ITU	International Telecommunications Union
JRC	Joint Radio Committee
Km	Kilo meters
LDT	location Determination Technologies
LMS	Least Mean Squares
LMU	Location Measurement Units
LOS	Line Of Sight

LTE	Linear Transversal Equalizer
MAP	Maximum Aposteriori Probability
MDE	Mean Distance Error
MLP	Multi-Layered Perceptron
MLSE	Maximum Likelihood Sequence Estimator
MLVA	Maximum Likelihood Viterbi Algorithm
MS	Mobile Station
NLOS	Non-Line of Sight
NMR	Network Measurement Results
PAM	Pulse Amplitude Modulation
PCS	Personal Communication Systems
PSTN	Public Switched Telephone Network
QAM	Quadrature Amplitude Modulation
RBF	Radial Basis Function
RF	Radio Frequency
RLS	Recursive Least Squares
RX	Receiver
SIR	Signal-to-Interference Ratio
SS	Spread Spectrum
TA	Timing Advance
TDOA	Time Difference of Arrival
TOA	Time of Arrival
T-R	Transmitter – Receiver
TWNE	Transversal Wavelet Network-based Equalizer
UHF	Ultra high Frequency
UTD	Uniform Theory of Diffraction
VHF	Very High Frequency
WCDMA	Wideband Code Division Multiple Access
WIM	Walfisch-Ikegami Model

Chapter 1

1 Introduction

This thesis presents neural network based approaches for tackling two important problems encountered in cellular networks, namely prediction of mobile locations and co-channel interference suppression.

The prediction of a mobile location using propagation path loss (signal strength) is a very difficult and complex task. The accuracy depends on the environment (Multipath, NLOS, shadowing), path loss model used, number of base stations used and techniques such as Enhanced Observed Time Difference (E-OTD), Global Positioning System (GPS), A-GPS (Assisted-GPS), Cell ID, Timing Advance (TA), Time of Arrival (TOA), Angle of Arrival (AOA), Time Difference of Arrival (TDOA) and signal strength based techniques for estimating the cellular phone position are used.

Several techniques have been proposed recently mostly based on linearized, geometrical and maximum likelihood methods. An alternative approach based on artificial neural networks is proposed in this thesis which offers the advantages of increased flexibility to adapt to different environments and high speed parallel processing. The research presented in this thesis gives an overview of conventional location estimation techniques and the various propagation models reported to-date, and a new signal-strength based neural network technique is then described. A simulated mobile architecture based on the realistic COST-231 Non-line of Sight (NLOS) Walfisch-

Ikegami implementation of a metropolitan environment is first used to assess the generalization performance of an Artificial Neural Network (ANN) based mobile location predictor. Limited real data is then used to further evaluate the performance of the ANN mobile location predictor with promising initial results. The performance of two ANNs, namely the Multi-Layered Perceptron (MLP) and a Radial Basis Function (RBF) based network, is compared with a conventional linear adaptive filtering approach for both simulated and real environment data.

Secondly, this thesis presents a brief overview and comparative performance evaluation of selected neural network based equalizers for the problem of co-channel interference suppression in cellular networks. The problem of adaptive equalization of digital communication channels in the presence of Inter-Symbol Interference (ISI), additive white gaussian noise (AWGN) and co-channel interference is first reviewed and a realistic co-channel system is then used as a case study to show that neural network based Decision Feedback equalizers exhibit superior Bit Error Rate (BER) performance characteristics compared to the conventional Linear Transversal Equalizer (LTE) and the conventional linear DFE. The sample results in this study have considered single co-channel systems, but they can be extended to the multi-co-channel case.

1.1 *Background and Context*

1.1.1 Location Estimation in Cellular Networks

Location Estimation is the process of localizing an object on the basis of some parameter. This parameter can be proximity to a detector, or some other parameter like radiated energy. The latter parameter is the one of interest in our case. In the particular

context of cellular systems, this translates to the localization of the transmitter or the receiver.

Proper location estimation is very important in making many crucial decisions in cellular networks. Handoff management is one such example. When a mobile station enters from the region of service of one BS to another, a handoff is to be made. The initiation of the handoff process depends on the location of the mobile. A delay in the initiation of handoff will result in very low signal strength or in the adverse case, a call drop. Applications like handoff management don't require very accurate location estimates; all that is required is to determine which cell the mobile is in. But there are applications that ask for a very accurate estimate [1].

1.1.2 Co-channel interference Suppression in Cellular Networks

Many digital communications systems employ frequency reusage and often exhibit performance limitation due to co-channel interference [49]. Frequency reuse is referred to the employment of radio channels on the same carrier frequency to cover different areas or cells situated sufficiently apart from one another, and allow cellular radio systems to handle far more simultaneous calls than the total number of allocated channel frequencies. Signals from co-channel cells (i.e. cells of the same channels frequency) will however interfere with each other. The degradation in quality due to co-channel interference is often more severe than that caused by additive noise or Inter-symbol interference (ISI) [50].

1.2 *Motivation*

Localising handset users within a mobile network has always been seen as an important capability, since its successful incorporation would allow crucial services to be delivered to customers. These services include effective handling of emergency calls, location sensitive billing and intelligent transportation. The problem of estimating mobile location is now receiving significant attention ever since the U.S. Federal Communication Commission (FCC) made it mandatory for network operators to be able to locate users with demanding requirements on the location accuracy. At present conventional location determination technologies (LDTs) fall into two main classes [51], namely handset-based and network bases LDT's. Currently, GPS based location information services are in commercial use - when accurate signal strength measurements from at least three Base Stations are available, geometrical (triangulation) methods are used to determine the two-dimensional (2-D) location co-ordinates of the mobile user. However, in a city or building where there is often no direct Line of Sight (LoS) between GPS satellite and the terminal, this causes a severe degradation of accuracy. In such cases, location estimation using cellular network systems can offer advantages, and estimating a location using the signal from BS's becomes a highly non-linear problem. Few linearized and geometrical methods have been proposed for calculating the mobile position based on measured signal strengths [52]. Although signal strength based location estimation algorithms may not be the preferred approach at present (commercially) for providing location services, signal strength is the only common attribute available between various kinds of mobile networks and deserves more attention than received to-date. One principal reason for

this is the ability of signal strength measurements to provide network-based mobile location solutions without the need to modify the handsets. The motivation behind the proposed application of neural networks to solve the location estimation problem is that the neural network technique is adept to the use of intelligence in the cellular system. Also, the inherent nature of the location estimation problem makes neural nets selection a wise choice for tackling this problem. Modelling the propagation of radio waves by mathematical models is quite complex involving numerous interacting variables. In addition, multipath, diffraction and non line of sight (NLOS) cause problems. Also weather conditions affect the radio wave propagation. In this research, the application of neural networks is considered as a function approximation problem [2, 3] consisting of a non-linear mapping of signal strength input (received at several Base Stations) onto a dual output variable representing the mobile location co-ordinates.

On the other hand, the choice of neural networks for co-channel interference suppression is motivated by the growing need to exploit the use of new neural network structures as non-linear adaptive filters in the telecommunications industry. With the present great demand for data communication services, bit rates and symbol rates are being pushed towards their theoretical limits. Consequently, communication channel impairments that previously went unnoticed can be particularly problematic [59]. – for example, when transmitting the data over PSTN (Public Switched Telephone Network) at moderate bit rates, the channel can be considered to be linear; however, at high bit rates, the non-linearities introduced by the network elements such as the coupling transformers, codecs and amplifiers cannot be ignored, and must be compensated for by

the use of appropriate non-linear signal processing techniques [43], [44]. Conventional neural network based adaptive non-linear equalizers have excessive computational requirements and require relatively large training periods in order to realise the optimal equalization performance [43, 45-47]. Hence, new faster and computationally efficient neural network equalizers need to be developed which can better compensate for not only the linear and non-linear communication channel distortion, but additionally also be able to suppress other significant interference factors such as co-channel interference effects, encountered in many digital communications systems, for example, digital cellular radio (DCR) [48]. As stated earlier, the degradation in quality due to co-channel interference is often more severe than that caused by the additive noise or ISI [50]. In land mobile radio systems for instance, geographical frequency reuse is used to provide a system with a high traffic carrying capacity, using a limited amount of radio spectrum. The extent to which frequencies can be reused is limited by the tolerance of the receiver to co-channel interference. The traffic capacity of the system is directly linked to the extent of frequency reuse, and consequently to a receiver's ability to combat co-channel interference. The optimal solution to the problem assumes perfect knowledge of the mobile environment. As the mobile environment is unknown and can change, adaptive equalizers are therefore required in these communications systems in order to achieve an acceptable error-rate performance [48].

1.3 *Original Contributions*

The main thesis contributions are:

- Novel application of two specific neural network models, namely the feedforward Multi-Layered Perceptron (MLP), and the Radial Basis Function (RBF) based generalized regression neural network (GRNN) in order to predict the location of a mobile user using the signal strength data obtained from both a simulated COST-231 and a real urban environment. For the case of the simulated data, generated using the COST-231 model (which is often used by the deigners of public mobile radio systems) the MLP based mobile location predictor was found to perform better than both the GRNN and a linear predictor in terms of the mean distance error (MDE) performance measure but at the cost of an increased computational requirement. A reduction in the training data achieved by reducing the number of simulated base stations (BS) from three to two was found to have minimal detrimental effect on the MDE performance measure of both the neural location predictors. The MDE performance of the neural predictors was also evaluated using very limited real data provided by a UK telecommunications company (for a small UK town), and both the neural predictors were found to produce highly accurate location predictions for the case of data from three BSs compared to the linear predictor. Finally, simulation results were used to demonstrate that both the neural predictors are capable of providing reasonably accurate location estimates even in the case of more limited real data from just two BSs.

- Secondly, this thesis had presented a new comparative performance evaluation of selected neural network based adaptive equalizers, namely the RBF, wavenet and Functional-link neural networks, in overcoming co-channel interference in cellular networks. A realistic co-channel system is used as a case study to demonstrate the equalization capability of the neural network based equalizers. The results demonstrate superior Bit Error Rate (BER) performance characteristics for the functional-link neural network based decision feedback equalizer (DFE), compared to other conventional linear and neural network based adaptive equalizers. The results in this study have considered single co-channel systems, but they can be extended to the multi-co-channel case.

1.4 *Publications*

The following papers have resulted from this research:

1. J. Muhammad, A. Hussain & W. Ahmad, "*Location Estimation in Cellular Networks using Neural Networks*", Proceedings 1st IEEE-IEE-ESF International Workshop on Signal Processing for Wireless Communication (SPWC'2003), pages 243-247, King's College, London, 19-20 May, 2003

2. J. Muhammad, A. Hussain & W.Ahmed, "*New Neural Network based Mobile Location Estimation in Urban Propagation Models*", Proceedings 7th IEEE International Multi-Topic Conference (INMIC'2003), Islamabad, 8-9 Dec, 2003.

3. J. Muhammad, A. Hussain, Alexander Neskovic & Evan Magill, "*New Neural Network Based Mobile Location Estimation in a Metropolitan Area*", **Book Chapter**, in Lecture Notes in Computer Science (LNCS), Springer Berlin / Heidelberg, ISSN: 0302-9743, Volume 3697/2005, pages 935-941, Artificial Neural Networks: Formal Models and Their Applications - ICANN 2005 , ISBN: 978-3-540-28755-1

The following paper is in preparation.

4. J. Muhammad, A. Hussain, “Comparative Evaluation of Neural Network based Adaptive Non-linear Equalizers for Overcoming Co-channel Interference”

1.5 *Thesis Organisation*

The thesis is divided into 6 chapters.

- Chapter 2 presents an overview of radio wave principles and various propagation models reported to-date.

- Chapter 3 discusses and critically evaluates the predominant location estimation techniques in use.

- Chapter 4 gives an overview of a few selected conventional neural network paradigms, including the most widely used feedforward Multi Layer Perceptron (MLP), and the Radial Basis Function (RBF) based Generalized Regression Neural Network (GRNN), and then describes their novel use for location estimation in cellular networks. Simulation results are presented assessing the generalization performance of neural network based location predictors and compared with a linear adaptive filtering based approach. Preliminary findings using real data are also presented and discussed.

- Chapter 5 gives an overview of the co-channel interference problem in cellular networks, including the conventional approaches that have been developed to-date. Following this, a discrete time model for a Digital Cellular Radio (DCR) system is presented and simulation results are used to demonstrate the application of selected neural network based equalizers to a realistic co-channel system and their BER performance characteristics compared.

- Finally, chapter 6 presents some concluding remarks and future work proposals.

Chapter 2

2 Review of Mobile Radio Systems' Propagation Models

The mobile radio channel places fundamental limitations on the performance of wireless communication systems. The transmission path between the transmitter and the receiver can vary from simple line-of-sight to one that is severely obstructed by buildings, mountains, and foliage. Unlike wired channels that are stationary and predictable, radio channels are extremely random and do not offer easy analysis. Even the speed of motion impacts how rapidly the signal level fades as a mobile terminal moves in space.

Radio wave propagation has historically been the most difficult problem to analyze and design for, since unlike a wired communication system which has a constant, stationary transmission channel (i.e., a wired path), radio channels are random and undergo shadowing and multipath fading, particularly when one of the terminals is in motion.

This chapter gives an overview of radio wave propagation, principles, factors affecting the propagation and a brief review of the most commonly used outdoor and indoor propagation models.

2.1 Radio Wave Propagation

With location estimation systems based on radio signals, it is important to know the propagation properties of electromagnetic radiation. Phenomena, such as signal attenuation, reflection, scattering and diffraction have important roles in location

estimation. Their importance is emphasized in non-satellite systems which have to operate in complex propagation environments, such as urban or mountainous areas. This chapter addresses the most important theoretical aspects of radio wave propagation and reviews some propagation models based on them.

2.2 *Principles*

The basic concept in the theory of electromagnetic radiation is an *electric field*, which is always related to electric current [4]. An electric field E is defined by its direction and magnitude at each point. The magnitude, denoted by $|E|$, is measured in units of volts per meter (V/m). Periodic fluctuations of an electric field are called *radio waves*. Radio waves can be decomposed in orthogonal components, typically the horizontal and the vertical component. The ratio of the magnitudes of the two components - or equally: the direction of the electric field - defines the *polarization* of the wave [5]. For instance, if the magnitude of the vertical component is always zero, i.e. the direction vector is always parallel to the horizontal axis, the wave is said to be horizontally polarized.

An electric field corresponds to a *power density* flow F, measured in watts per square meter (W/m^2), which is proportional to the square of the magnitude of the electric field. Given the power density flow, the gain of a receiving antenna, G_r, which depends on the physical size of the antenna and frequency, the wave length λ, and the system hardware loss, L, the received power is given by,

$$P_R = \frac{FG_r\lambda^2}{4\pi L} \qquad (2.1)$$

Even though the wave length λ appears in Equation (2.1), it does not follow that the received power would increase proportionally to the square of the wave length, because the wave length also affects the gain of the receiving antenna G_r. In fact, if the physical size of the antenna and the power density flow are constant, the wave length terms cancel each other out, and thus the received power is independent of the frequency. However, the frequency can indeed affect the power density flow due to interactions with the propagation medium. This issue will be discussed in the following sections.

Because the values of received power vary over a wide range, it is convenient to use logarithmic scale. A ratio of two quantities can be presented in decibels (dB) which indicates the logarithm of the ratio multiplied by ten. The unit of decibel watt (dBW) is the ratio of power referenced to one watt. Conversions between watts and decibel watts are made with the following two equations:

$$P[dBW] = 10\log_{10}(P[W]) \qquad (2.2)$$

$$P[W] = 10^{\frac{P[dBW]}{10}} \qquad (2.3)$$

For instance, 0 dBW is equal to one watt, 10 dBW is equal to 10 watts, 20 dBW is equal to 100 watts, etc. The unit of decibel milliwatt (dBm) is defined similarly as the ratio of power referenced to one milliwatt. Conversions between two decibel units, for instance, decibel watts and decibel milliwatts, can always be performed simply by adding a

constant to the original value. The following two equations are used for converting decibel watts to decibel milliwatts and *vice versa*:

$$P[dBm] = P[dBW] + 30 \tag{2.4}$$

$$P[dBW] = P[dBm] - 30 \tag{2.5}$$

2.2.1 Free-space Attenuation

Because a wave front proceeds in three dimensions, the maximum received power at distance d must decrease in the inverse of the area of a sphere with radius d. If the absorption loss of the propagation medium is ignored, the power density flow, F, is given by

$$F = \frac{P_T G_T}{4\pi d^2} \tag{2.6}$$

where P_T is the transmitted power, G_T is a factor depending on the transmitting antenna, and d is the distance [6,7]. Combining Equations (2.1) and (2.6) gives the received power, which is usually given in decibels:

$$P_R[dB] = P_T[dB] + 10\log(G_T) + 10\log(G_R) + 20\log(\lambda) - 20\log(d) - 22.0 \tag{2.7}$$

Equations (2.6) and (2.7) are valid only in free-space environment. If the line-of-sight between the transmitter and the receiver is obstructed, the received signal power is

significantly lower than the free-space equations suggest and they do not necessarily give a good approximation.

Wave propagation depends on several phenomena such as absorption, reflection, diffraction and scattering.

2.2.2 Absorption (or penetration)

In any real-world communication system, the signals propagate in some medium. In wireless terrestrial systems the medium is mainly the atmosphere and, in lesser degree, materials such as glass, concrete, wood, etc. Due to interactions with the medium, the signal loses a certain proportion of its remaining energy on every unit of distance it propagates. Thus, absorption causes the power density flow to decrease proportionally to γ^{-d}, where d is the distance, and γ is a constant depending on the properties of the medium and signal frequency. This means that in decibel scale, the loss is linear with respect to the distance.

Absorption loss is particularly great in the upper microwave region, where the frequencies are above 10 GHz. With these frequencies the absorption due to atmosphere becomes comparable to the free-space attenuation, especially in heavy rain conditions and with long transmitter-receive distances [8]. With frequencies used in most wireless communication systems, below 10 GHz, the atmospheric absorption is insignificant with distances up to 10 km.

Absorption caused by other media than air is generally very strong. Moreover, in addition to absorption, obstructions cause the wave to be reflected, which further decreases the amount of energy passing through. Taking into account both reflection and absorption, the total attenuation per obstruction is typically 1-20 dB below 10 GHz, and 1-60 dB above 10 GHz [6].

2.2.3 Reflection

Reflection occurs when a wave meets an obstacle with size much bigger than the wave length. The part of the wave that is not reflected back loses some of its energy by absorbing to the material and the remaining part passes through the reflecting object. In terrestrial communication systems the waves usually reflect from ground, producing a two-ray path between the transmitter and the receiver, shown in figure 2.1. The *plane of incidence* is defined as the plane containing both the incident ray and the reflected ray, and the *angle of incidence* is the angle between the reflecting surface and the incident ray.

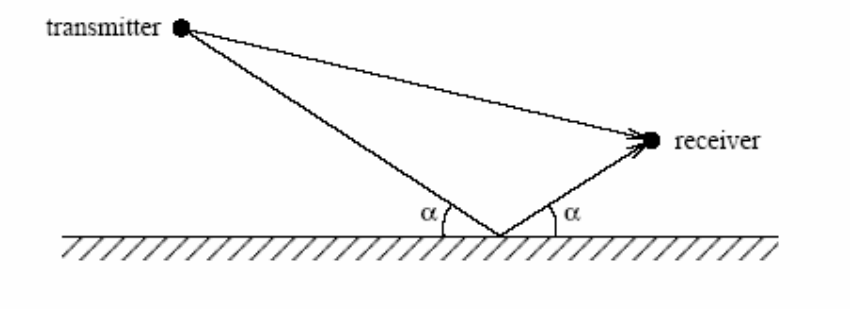

Figure 2.1: Two-ray ground reflection model

The received signal consists of the direct line-of-sight ray and the reflected ray. The two rays arriving to a receiver can have different phase and in the worst case they cancel

each other out. The magnitude of the reflected signal depends on the *Fresnel reflection coefficient,* which depends on the properties of the reflecting ground, the frequency of the wave, and the angle of incidence. Roughness of the reflecting surface causes the propagating waves to *scatter* in all directions, and therefore, the reflection coefficient of a rough surface is smaller than the one of an otherwise identical but flat surface. In general, the reflection coefficient is different for the vertical and the horizontal component of the wave. In such cases, reflection can change wave polarization.

Figure 2.2 presents the attenuation curve of the two-ray model with certain parameters. The exact equation corresponding to the two-ray model is given in [6]. It can be seen from the figure that with long distances the two-ray model coincides with the *fourth-power approximation,* which is given by

$$P_R[dB] = P_T[dB] + 10\log(G_T) + 10\log(G_R) - 40\log(d) - 22.0 \qquad (2.8)$$

where the received power is proportional to the inverse of the fourth power of the distance rather than the square of the distance which appears in the free-space model.

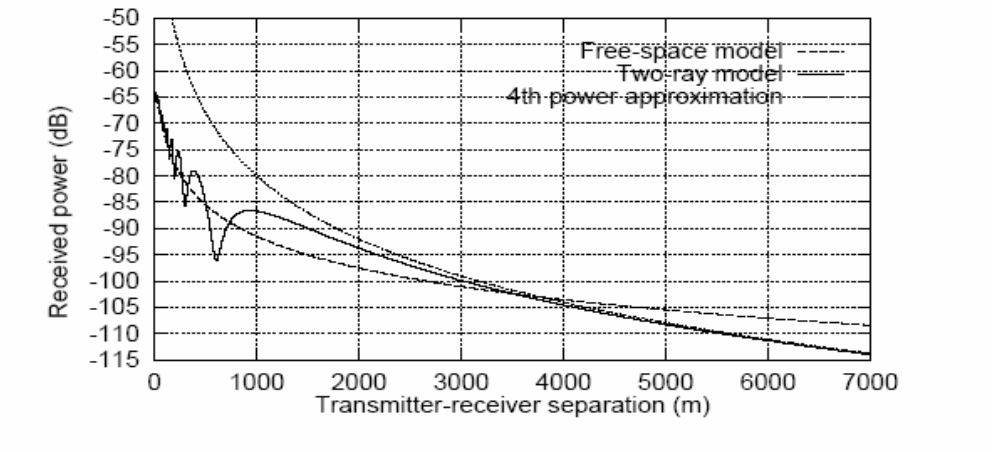

Figure 2.2: The received power referenced to the transmitted power

The received power referenced to the transmitted power as a function of the transmitter-receiver distance according to the free-space model (Equation (2.7)), the two-ray model [6], and the fourth-power approximation of the two-ray model (Equation (2.8)). The parameters are: transmitter elevation = 50 m, receiver elevation = 2 m, frequency = 900 MHz, relative permittivity of the ground = 15, antenna gains and system loss = 1.0 (no loss).

2.2.4 Diffraction

According to Huygen's principle, all points on a wavefront are point sources of secondary waves propagating to all directions. Therefore, each time a radio wave passes an edge such as a corner of a building the wave "bends" around the edge and continues to propagate into the area shadowed by the edge. This effect is called *diffraction* [72]. In Figure 2.3 the transmitter is situated near an obstacle. The arrows describing the direction of propagation indicate how the signal reaches the areas around the corner due to a source of secondary waves situated at the corner of the obstacle. Note that the

single source of secondary waves shown in Figure 2.3 is only one of the infinite numbers of such sources on the wavefront.

The more the waves have to bend around a corner, the more they lose their energy. Therefore the areas to which the rays have to bend more, gain relatively less additional field strength than the areas to which the rays can proceed almost linearly. The field strength of the secondary waves is much smaller than the one of the primary waves. In practice the diffracted waves can be neglected if there is a line-of-sight between the transmitter and the receiver.

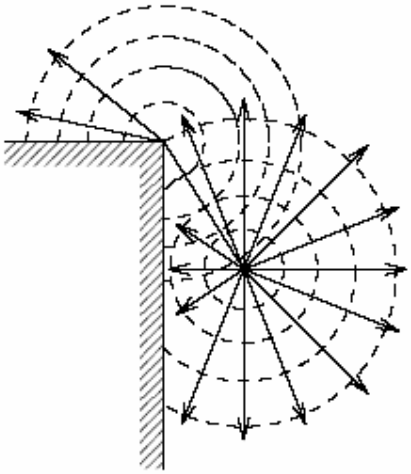

Figure 2.3: Diffraction

2.2.5 Scattering

Scattering phenomena occurs when the medium through which the wave travels is composed of objects with small dimensions, when compared to the wavelength, and where the number of obstacles is large. Scattered waves are produced when waves impinge on rough surfaces, foliage and small objects in general [9].

2.3 *Propagation Models*

A propagation model is a set of mathematical expressions, diagrams, and algorithms used to represent the radio characteristics of a given environment. Generally, the prediction models can be either empirical (also called statistical) or theoretical (also called deterministic), or a combination of these two. While the empirical models are based on measurements, the theoretical models deal with the fundamental principles of radio wave propagation phenomena.

In the empirical models, all environmental influences are implicitly taken into account regardless of whether they can be separately recognized. This is the main advantage of these models. On the other hand, the accuracy of these models depends not only on the accuracy of the measurements, but also on the similarities between the environment to be analyzed and the environment where the measurements are carried out. The computational efficiency of these models is usually satisfying.

The deterministic models are based on the principles of physics and, due to that; they can be applied to different environments without affecting the accuracy. In practice, their implementation usually requires a huge database of environmental characteristics, which is sometimes either impractical or impossible to obtain. The algorithms used by deterministic models are usually very complex and lack computational efficiency. For that reason, the implementation of the deterministic models is commonly restricted to smaller areas of microcell or indoor environments. Nevertheless, if the deterministic

models are implemented correctly, greater accuracy of the prediction can be expected than in the case of the empirical models.

On the basis of the radio environment, the prediction models can be classified into two main categories, outdoor and indoor propagation models. Further, in respect of the size of the coverage area, the outdoor propagation models can be subdivided into two additional classes, macrocell and microcell prediction models as shown in Figure 2.4 [10, 72].

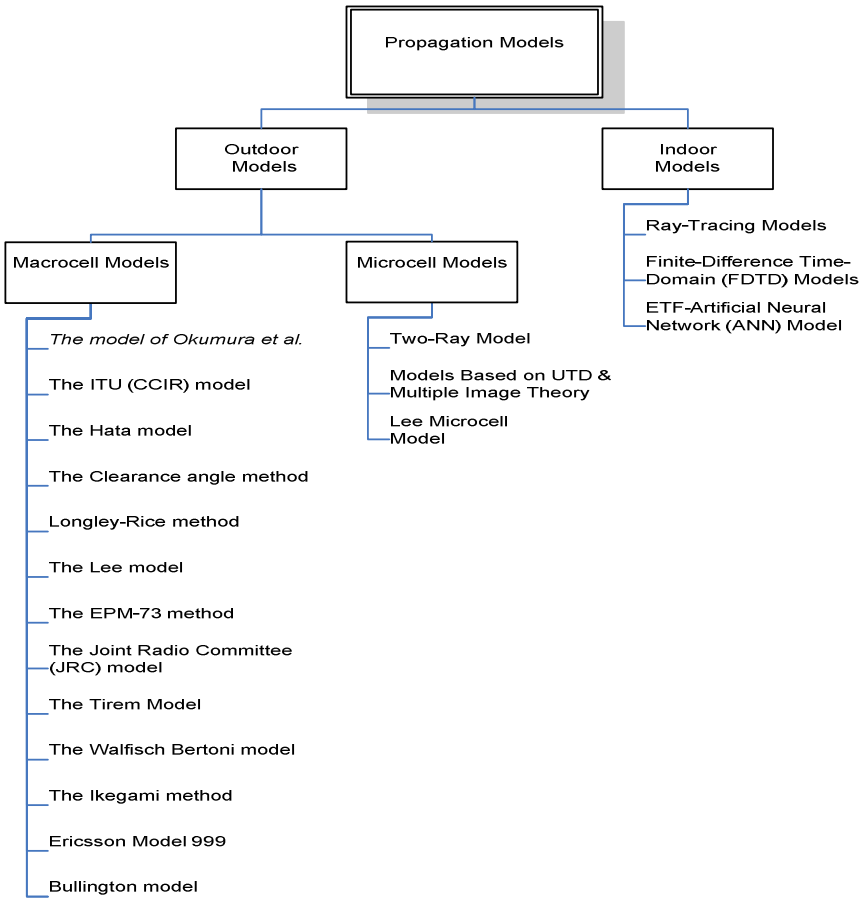

Figure 2.4: Classification of Propagation Models developed to-date

2.4 *Macrocell Propagation*

Macrocell design philosophy is based on the assumptions of high radiation centrelines, usually placed above the surroundings; transmitter powers on the order of several tens of Watts; and large cells whose dimensions are on the order of several tens of kilometers. Under these assumptions, LoS conditions are usually not satisfied and the signal from the transmitter to the receiver propagates by means of the diffraction and the reflection. Also, for large cells the effects of refraction are very important. All of these factors make the problem of field strength prediction very difficult. For years, a large number of researchers have been struggling with this problem. As a result a large number of models have been proposed [75]. Few of these models are mentioned in figure 2.4.

2.5 *Microcell Propagation*

A microcell is a relatively small outdoor area such as a street with the base station antenna below the rooftops of the surrounding buildings. The coverage area is smaller compared to macrocells and it is shaped by surrounding buildings. A microcell enables an efficient use of the limited frequency spectrum and it provides a cheaper infrastructure. The main assumptions are relatively short radio paths (on the order of 200m to 1000m), low base station antennas (on the order of 3m to 10m), and low transmitting powers (on the order of 10mW to 1W). Today, microcells are very often used in IS-95, PCS, DCS, GSM, DECT, etc.

There are many prediction models for a microcell situation such as Two-Ray model, Models based on UTD and multiple image theory, Lee microcell mode etc. [10].

2.6 *Indoor Propagation*

The indoor radio channel differs from the traditional mobile radio channel in two aspects – the distances covered are much smaller, and the variability of the environment is much greater for a much smaller range of T-R separation distances. It has been observed that propagation within buildings is strongly influenced by specific features such as the layout of the building, the construction materials, and the building type.

Indoor radio propagation is dominated by the same mechanisms as outdoor: reflection, diffraction, and scattering. However, conditions are much more variable. For example, signal levels vary greatly depending on whether interior doors are open or closed inside a building. Where antennas are mounted also impacts large-scale propagation. Antennas mounted at desk level in a partitioned office receive vastly different signals than those mounted on the ceiling. Also, the smaller propagation distances make it more difficult to insure far-field radiation for all receiver locations and types of antennas [6, 72]. Few examples of indoor models are; Ray-Tracing models, Finite-Difference Time-Domain (FDTD) Models, ETF-Artificial Neural Network (ANN) model etc.

Only a few very popular outdoor (macrocell and microcell) and indoor models like Okumura model, ITU (CCIR) model, Hata Model, Walfisch Ikegami model, Walfisch Bertoni model, Ray-Tracing (indoor propagation model) and Two-Ray Models

(Microcell model) are discussed here. The details of the other models could be found in [11-20].

2.6.1 Okumura Model

The Okumura *et al.* method [21] is based on empirical data collected in detailed propagation tests over various situations of an irregular terrain and environmental clutter. The results are analyzed statistically and compiled into diagrams. The basic prediction of the median field strength is obtained for the quasi-smooth terrain in the urban area. The correction factor for either an open area or a suburban area should be taken into account. The additional correction factors, such as for a rolling hilly terrain, the isolated mountain, mixed land-sea paths, street direction, general slope of the terrain etc., make the final prediction closer to the actual field strength values. In the present engineering practice, the Okumura *et al.* method is widely used. This is a method originally intended for VHF and UHF land-mobile radio systems and involves neither complex computations nor an elaborate theory. Much of its experimental data have been incorporated in the ITU (CCIR) reference curves as well as in other popular models.

However, many authors [13, 22, and 23], show certain reserve toward the application of the Okumura model. They note that extensive data regarding its performance must be obtained before its use may be advocated. In addition, more careful interpretation of the definitions of various parameters needs to be made. When assessing the values of the model's parameters, the influence of the subjective factors is not easy to avoid, thus yielding different results for the same problem.

In order to make the Okumura technique suitable for computer implementation, Hata has developed the analytic expressions for the medium path loss for urban, suburban, and open areas [24, 25]. Although these expressions are only approximations and therefore have some limitations, they are almost always used in practice instead of the basic Okumura curves.

2.6.2 ITU (CCIR) Model

An empirical formula for the combined effects of free-space path loss and terrain-induced path loss was published by the CCIR (Comité Consultatif International des Radio-Communication, now ITU-R) and is given by [26]

$$\begin{aligned} L(dB) = 69.55 + 26.16\log_{10} f_{MHz} - 13.82\log_{10} h_1 - a(h_2) \\ +(44.9 - 6.55\log_{10} h1)\log_{10} d_{km} - B \end{aligned} \qquad (2.9)$$

where h_1 and h_2 are base station and mobile antenna heights in meters, respectively, d_{km} is the link distance in kilometres, f_{MHz} is the centre frequency in megahertz, and

$$\left.\begin{aligned} a(h_2) &= (1.1\log_{10} f_{MHz} - 0.7)h_2 - (1.56\log_{10} f_{MHz} - 0.8) \\ B &= 30 - 25\log_{10}(\%\, of\ area\ \mathrm{cov}ered\ by\ buildings) \end{aligned}\right\} \qquad (2.10)$$

This formula is the Hata model for medium-small city propagation conditions, supplemented with a correction factor, B. The term B is such that the correction B = 0 is

applied for an urban area, one that is about 15% covered by buildings; for example, if 20% of the area is covered by buildings, then $B = 30 - 25\log_{10} 20 = -2.5dB$

2.6.3 Hata Model

The Hata model is an empirical formulation of the graphical path loss data provided by Okumura, and is valid from 150 MHz to 1500 MHz. Hata presented the urban area propagation loss as a standard formula and supplied correction equations for application to other situations. The standard formula for median path loss in urban areas is given by

$$L_{50}(Urban)(dB) = 69.55 + 26.16\log f_c - 13.82\log h_{te} - a(h_{re}) + (44.9 - 6.55\log h_{te})\log d \qquad (2.11)$$

where f_c is the frequency (in MHz) from 150 MHz to 1500 MHz, h_{te} is the effective transmitter (base station) antenna height (in meters) ranging from 30 m to 200 m, h_{re} is the effective receiver (mobile) antenna height (in meters) ranging from 1 m to 10 m, d is the T-R separation distance in km, and $a(h_{re})$ is the correction factor for effective mobile antenna height which is a function of the size of the coverage area. For a small to medium sized city, the mobile antenna correction factor is given by

$$a(h_{re}) = (1.1\log f_c - 0.7)h_{re} - (1.56\log f_c - 0.8)\ dB \qquad (2.12)$$

and for a large city, it is given by

$$\left.\begin{aligned} a(h_{re}) &= 8.29(\log 1.54h_{re})^2 - 1.1dB, \quad for\ f_c \le 300\,MHz \\ a(h_{re}) &= 3.2(\log 11.75h_{re})^2 - 4.97\,dB, \quad for\ f_c \ge 300\,MHz \end{aligned}\right\} \qquad (2.13)$$

To obtain the path loss in suburban area the standard Hata formula in equation (2.11) is modified as

$$L_{50}\,(dB) = L_{50}\,(Urban) - 2[\log(f_c / 28)]^2 - 5.4 \qquad (2.14)$$

For path loss in open rural areas, the formula is modified as

$$L_{50}\,(dB) = L_{50}\,(urban) - 4.78(\log f_c)^2 - 18.33 \log f_c - 40.98 \qquad (2.15)$$

Although Hata's model does not have any of the path-specific corrections which are available in Okumura's model, the above expressions have significant logical value. The prediction of the Hata model compare very closely with the Okumura model, as long as *d* exceeds 1 km. this model is well suited for large cell mobile systems, but not personal communication systems (PCS) [6].

2.6.4 COST 231 –Walfisch Ikegami Model

In Europe, research under the Cooperation in the field of Scientific and Technical Research (COST) program has developed improved empirical and semi deterministic models for mobile radio propagation [27]. In particular, Project 231 (COST 231), entitled "Evolution of Land Mobile Radio Communications", resulted in the adoption of propagation modelling recommendations for cellular and PCS applications by the International Telecommunications Union (ITU), including a semi-deterministic model for medium-to-large cells in built-up areas that is called the Walfisch-Ikegami model [28]. This model (WIM) has been shown to be a good fit to measured propagation data for frequencies in the range of 800 to 2,000 MHz and path distances in the range of 0.02 to 5 km. The COST 231-Walfisch-Ikegami model (COST 231-WI) [29] has been used

extensively in typical suburban and urban environments where the building heights are quasi-uniform. The designers of the public mobile radio systems (e.g., GSM, PCS, DECT, DCS, etc.) often use this model [10].

The WIM distinguishes between LOS and non-line-of-sight (NLOS) propagation situations. In a LOS situation, there is no obstruction in the direct path between the transmitter and the receiver, and the WIM models the propagation loss in dB by the equation

$$L_{LOS} = 42.64 + 26\log_{10} d_{km} + 20\log_{10} f_{MHz},\ d_{km} \geq 0.02 \qquad (2.16)$$

Note that the propagation law (power of distance) for the LOS situation is modelled as being 26/10 = 2.6, so that $L_{LOS} \propto d^{2.6}$. This model assumes that the base station antenna height (≥ 30m) ensures that the path has a high degree of fresnel zone clearance. The propagation loss in free space is given by

$$L_{fs} = 32.45 + 20\log_{10} d_{km} + 20\log_{10} f_{MHz} \qquad (2.17)$$

The LOS propagation loss can be written as

$$\begin{aligned} L_{LOS} &= L_{fs} + 10.19 + 6\log_{10} d_{km} = L_{fs} + 6\log_{10}(50\, d_{km}) \\ &= L_{fs} + 6\log_{10}(d_m / 20) \end{aligned} \qquad (2.18)$$

where d_m is the distance in meters.

For NLOS path situations, the WIM gives an expression for the path loss that uses the parameters illustrated in figure 2.5.

h_b = Base antenna height over street level, in meters (4 to50 m)

h_m = Mobile station antenna height in meters (1 to 3 m)

h_B = Nominal height of building roofs in meters

$\Delta h_b = h_b - h_B$ = Height of base antenna above rooftops in meters

$\Delta h_m = h_B - h_m$ = Height of mobile antenna below rooftops in meters

b = Building separation in meters (20 to 50m, if no data)

w = Width of street (b/2 recommended if no data)

φ = Angle of incident wave with respect to street (use 90° if no data),

d = Distance between transmitter and receiver (20...5000 m)

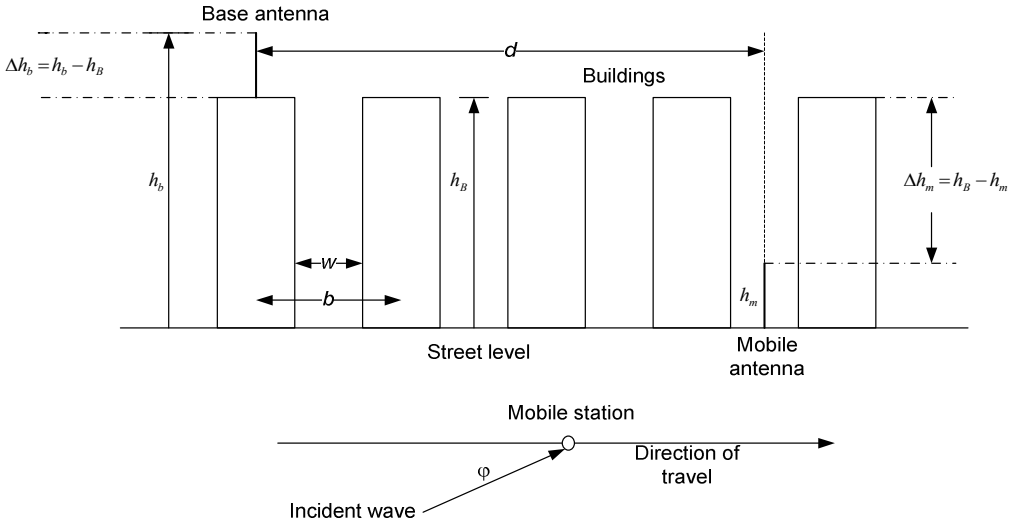

Figure 2.5: WIM NLOS parameters

In the absence of data, building height in meters may be estimated by three times the number of floors, plus 3m if the roof is pitched instead of flat. The model works best for base antennas well above the roof height.

Using the parameters listed above, for NLOS propagation paths the WIM gives the following expression for the path loss in dB:

$$L_{NLOS} = \begin{cases} L_{fs} + L_{rts} + L_{mds}, & L_{rts} + L_{mds} \geq 0 \\ L_{fs}, & L_{rts} + L_{mds} < 0 \end{cases} \quad (2.19)$$

where

$$L_{fs} = \text{Free-space loss} = 32.45 + 20\log_{10} d_{km} + 20\log_{10} f_{MHz} \quad (2.20)$$

L_{rts} = Roof-to-street diffraction and scatter loss (2.21)

L_{msd} = Multiscreen diffraction loss (2.22)

The loss terms L_{rts} and L_{msd} are functions of the NLOS parameters.

The formula given for L_{rts} involves an orientation loss, L_{ori};

$$L_{rts} = -16.9 - 10\log_{10} \omega + 10\log_{10} f_{MHz} + 20\log_{10} \Delta h_m + L_{ori} \quad (2.23)$$

where

$$L_{ori} = \begin{cases} -10 + 0.354\phi, & 0 \leq \phi \leq 35° \\ 2.5 + 0.075(\phi - 35°), & 35° \leq \phi \leq 55° \\ 4.0 - 0.114(\phi - 55°), & 55° \leq \phi \leq 90° \end{cases} \quad (2.24)$$

The formula given for the multi-screen diffraction loss term L_{msd} is

$$L_{msd} = L_{bsh} + k_a + k_d \log_{10} d_{km} + k_f \log_{10} f_{MHz} - 9\log_{10} b \quad (2.25)$$

In this expression, L_{bsh} is shadowing gain (negative loss) that occurs when the base station antenna is higher than the rooftops:

$$L_{bsh} = \begin{cases} -18\log_{10}(1+\Delta h_b), & \Delta h_b > 0 \\ 0, & \Delta h_b \le 0 \end{cases} \qquad (2.26)$$

L_{msd} decreases for wider building separation (b). The quantities k_a, k_d, and k_f determine the dependence of the loss on the distance (d_{km}) and the frequency (f_{MHz}). The term k_a in the formula for the multiscreen diffraction loss is given by

$$k_a = \begin{cases} 54, & \Delta h_b > 0 \\ 54 + 0.8\,|\Delta h_b|, & \Delta h_b \le 0 \; and \; d_{km} \ge 0.5 \\ 54 + 0.8\,|\Delta h_b|\,(d_{km}/0.5), & \Delta h_b \le 0 \; and \; d_{km} < 0.5 \end{cases} \qquad (2.27)$$

this relation results in a 54-dB loss term if the base station antenna is above the rooftops ($\Delta h_b > 0$), but more than 54 dB if it is below the rooftops. The increase from 54 dB is less if the link distance is rather small (less than 500m).

The distance factor k_d in the formula for L_{msd} is given by

$$k_d = \begin{cases} 18, & \Delta h_b > 0 \\ 18 + 15(|\Delta h_b| / h_B, & \Delta h_b \le 0 \end{cases} \qquad (2.28)$$

L_{msd} Increases with distance at 18dB/decade if the base antenna is above the rooftops ($\Delta h_b > 0$). But if the antenna is below the rooftops, the increase is higher (e.g., 30dB per decade when it is only 20% as high as the buildings ($\Delta h_b / h_B = 0.8$).

The frequency factor k_f in the formula for the multiscreen diffraction loss is given by

$$k_f = -4 + \begin{cases} 0.7\left(\frac{f_{MHz}}{925} - 1\right), \textit{medium city \& suburban} \\ 1.5\left(\frac{f_{MHz}}{925} - 1\right), \textit{metropolit a n..area} \end{cases} \quad (2.29)$$

L_{fs} and L_{rts} together give an increase of 30dB per decade of frequency. The expression for k_f indicates that this should be adjusted downwards for f < 6.21 GHz for medium city and suburban environments or f < 2.29 GHz for a metropolitan area [26, 73].

2.6.5 Walfisch and Bertoni model

A model developed by Walfisch and Bertoni considers the impact of rooftops and building heights by using diffraction to predict average signal strength at street level. It is a semi-deterministic model. The model considers the path loss, S, to be the product of three factors:

$$S = P_0 Q^2 P_1 \quad (2.30)$$

where *P*0 is the free space path loss between isotropic antennas given by

$$P_0 = \left(\frac{\lambda}{4\pi R}\right)^2 \quad (2.31)$$

The factor Q^2 reflects the signal power reduction due to buildings that block the receiver at street level. The P_1 term is based on diffraction and determines the signal

loss from the rooftop to the street. The model has been adopted for the IMT-2000 standard [6].

2.6.6 Two-Ray Model (Microcell model)

Numerous propagation models for microcells are based on a ray-optic theory. In comparison with the case of macrocells, the prediction of microcell coverage based on the ray-model is more accurate. One of the elementary models is the two-ray model. The two-ray model [30] is used for modelling of the LoS radio channel and is described in Fig. 2.6 below,

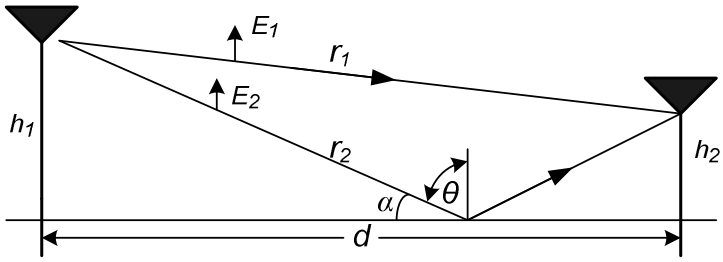

Figure 2.6: Two-Ray Model; the ray paths

The transmitting antenna of height h_1 and the receiving antenna of height h_2 are placed at distance d from each other. The received signal P_r for isotropic antennas, obtained by summing the contribution from each ray, can be expressed as:

$$P_r = P_t\left(\frac{\lambda}{4\pi}\right)^2\left|\frac{1}{r_1}\exp(-jkr_1)+\Gamma(\alpha)\frac{1}{r_2}\exp(-jkr_2)\right|^2 \qquad (2.32)$$

where P_t is the transmitter power, r_1 is the direct distance from the transmitter to the receiver, r_2 is the distance through reflection on the ground, and $\Gamma(\alpha)$ is the reflection coefficient depending on the angle of incidence α and the polarization.

The reflection coefficient is given by:

$$\Gamma(\theta)=\frac{\cos\theta - a\sqrt{\varepsilon_r - \sin^2\theta}}{\cos\theta + a\sqrt{\varepsilon_r - \sin^2\theta}} \tag{2.33}$$

where θ = 90°-α and a = 1/ε or 1 for vertical or horizontal polarization, respectively. ε_r is a relative dielectric constant of the ground.

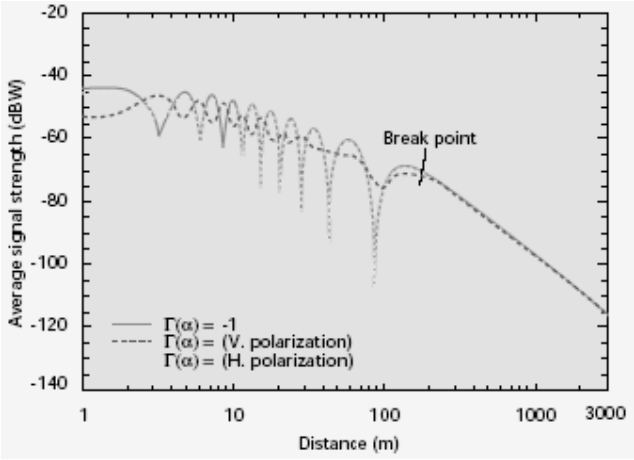

Figure 2.7: The receiving power, P_t= 1W, f=900MHz, h_1=8.7m and h_2=1.6m [30].

In Fig.2.7 above, the received power given by Eq. (2.32) is shown as a function of the distance for the cases of horizontal and vertical polarizations as well as for the case assuming Γ(θ) = -1. For large distances α is small, and Γ(θ) is approximately equal to - 1. For short distances, the value of Γ(θ) decreases and it can even be zero for vertical polarization.

Also, there are more complex models based on the ray-optic theory. The four-ray model consists of a direct ray, ground-reflected ray, and two rays reflected by buildings. The

six-ray model, besides the direct and the ground-reflected ray, takes four rays reflected by the building walls along the street. If a model considers a larger number of rays, the prediction tends to be more accurate, but the computational time is significantly increased. The problem deserving special attention is that of the corner diffraction. Two popular models considering this effect are the GTD (Geometrical Theory of Diffraction) model [31], and the UTD (Uniform Theory of Diffraction) model [32].

2.6.7 Ray-Tracing Model

The ray-tracing algorithm [20,31 and 32] calculates all possible signal paths from the transmitter to the receiver. In basic ray-tracing models, the prediction is based on the calculations of free-space transmissions and reflections from the walls. More complex ray-tracing algorithms include the mechanism of diffraction, diffuse wall scattering, and transmission through various materials. In the end, the signal level at any specific location is obtained as a sum of the components of all paths between the transmitter and the receiver. In addition to the propagation losses, the time dispersion of the signal can be successfully predicted by the ray-tracing models.

Today, the ray-tracing models belong to a group of the most accurate field strength prediction models. However, they require a very detailed layout of the area to be analyzed. The accuracy of the model depends on the accuracy and complexity of the area layout database. On the other hand, the implementation of these models requires extensive computational resources.

Ray-tracing algorithms can also be used for signal level prediction in outdoor environments, but for relatively smaller areas [10].

2.7 *Conclusions*

This chapter has presented an overview of radio wave principles and various propagation models reported to-date. The Walfisch-Ikegami model reviewed in this chapter is used for comparing the performance of our proposed neural network based location predictors in chapter 4.

The next chapter 3 discusses and critically evaluates the predominant location estimation techniques in use.

Chapter 3

3 Review of Location Estimation Methods

The location of mobile radios first appeared in military systems developed during the Second World War. The idea was simple: to find people in distress, or to detect and eliminate people causing distress. Location estimation is a process to identify the location of the caller by using various position determination technologies also known by terms such as radio location, radio navigation, position location, positioning, and so forth. The location can be expressed in different ways using different reference frames such as absolute spatial location, descriptive location, or relative location. The different ways of expressing location will pinpoint the location to certain point, area or region somewhere on or close to the earth. Another factor that affects the accuracy of the location is the use of location determination technology. A vast majority of applications of location estimation use the GPS satellite navigation system which provides location estimates with an accuracy of a couple of meters. However, in a city or building where there is often no direct Line of Sight (LoS) between GPS satellite and the terminal, this causes a severe degradation of accuracy. In such cases, location estimation using cellular network systems can offer advantages. The different techniques currently in use are discussed in this chapter.

3.1 *Location Determination Technologies*

Location Technologies mostly used by wireless carriers are handset-based and network-based [34]. These involve different levels of positional accuracy, hardware and software investment levels, and implications for the mobile operators. Few handset and network based technologies are described in the following sections.

3.1.1 Handset-based Location Technologies

In handset based location, the mobile station (MS) receives signals from the base stations (BS) and computes its own location. Few handset based location technologies are discussed below.

3.1.1.1 Cell-ID

Cell-ID operates in GSM, GPRS and WCDMA networks. It requires the network to identify the base station (BS) to which the cell phone is communicating and the location of that BS. The Cell-ID Location service identifies the mobile station (MS) location as the location of the Base Station and passes this information on to the location services application. Cell-ID was used earlier when high levels of location accuracy were neither mandatory nor necessary. If a handset is being used to make a call, then the information about the cell site that it is in will be updated to the network in real-time. However, if the handset is idle (i.e., switched on but not transmitting), then the last known transmission location will be stored by the network in the Home Location Register (HLR). In order to update the network's information on the location of a handset, the

network will page the device, prompting it to monitor the signal strength of the surrounding BS, thereby informing the network of its Cell ID.

The accuracy of this method depends on the cell size, and can be very poor in many cases, since typical GSM Cell is anywhere between 2km to 20km in diameter. With Pico cells, accuracy of 150 meters can be achieved. Using either one or both of the following techniques – Timing Advance (TA) and Signal Strength (RX Measurement/NMR), can increase the level of accuracy.

3.1.1.2 Cell-ID + Timing Advance (TA)

The time at which a terminal sends its transmission burst is critical to the efficient functioning of a GSM/GPRS network. Every mobile station within a given cell will be at a varying distance from the serving base station, yet the burst from each device must reach the base station at the exact moment that their receptive timeslots become available. Consequently, it is necessary for the mobile station to co-ordinate with the base station at the right time. Even though the burst arrive either before or after the availability of the allocated timeslot, the mobile station is instructed to “advance” the transmission of its burst accordingly. As the duration of the timing advance for each mobile station is dependent upon its distance from the base station, it is possible to use this information to determine how far away the caller is. TA information is only of any use in increasing the level of positioning accuracy within cells with a radius greater than 550 meters. This is because the adjustments made to the timing of the mobile station’s

transmissions are calculated depending on how many multiples of 500-550 meters the mobile station is distant from the base station.

3.1.1.3 Cell-ID + Signal Strength (RX Measurements)

The Mobile Station continuously measures the signal strength from each of the base station report this information back to the serving base station. This is so that the Mobile Station is able to transmit to – and receive from – the base station that has optimum signal strength, thereby improving the quality of call for the end user and making most efficient usage of network infrastructure. With this signal strength information, it is theoretically possible to calculate the position of the caller, by taking into consideration the rate at which the strength of an RX signal degrades as the distance between the transmitter and receiver increases. There are however number of factors that limit the effectiveness of this method, distance is not the only factor to affect RF waveform propagation. The characteristic of terrain between the transmitter and receiver, as well as the issue of indoor attenuation both has significant impact upon these measurements. The denser the material that a building is made from, as well as the higher the floor that a person is calling from, both have an increasingly negative affect on the strength of the signal received.

Signal Strength/RX measurements are sometimes referred to as Network Measurement Results (NMR) [35].

3.1.2 Network-Based Location Technologies

In network based techniques, base stations (BS's) receive signals from the mobile station (MS) and send the information to a control centre (CS) where the mobile stations location is computed.

3.1.2.1 Network based triangulation technologies

A number of different network-based measurement technologies can be used to locate a mobile user. Some of the major ones are described in the following section.

3.1.2.1.1 Enhanced Observed Time Difference (EOTD)

E-OTD operates only on GSM and GPRS networks. In GSM, the MS monitors transmission burst from multiple neighbouring BTSs and measures the time shifts between the arrivals of the GSM frames from the BTSs to which it is communicating. These observed time differences are the underlying measurement of the E-OTD radiolocation method and are used to trilaterate the position of the mobile devices. The accuracy of the E-OTD method is a function of the resolution of the time difference measurements, the geometry of Neighbouring Base station and the signal environment. The Mobile handset must measure time difference from at least three base stations to support two-dimension position determination (no altitude measurement is provided). E-OTD requires precise time information [35].

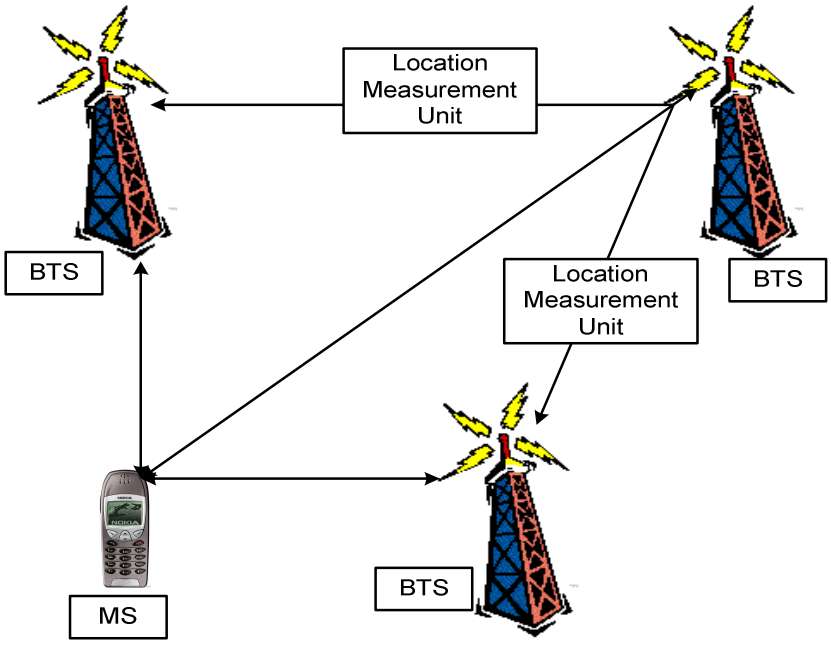

Figure 3.1: E-OTD Operations

Location Measurement Units (LMUs) is required in the GSM and GPRS network for precise time information. Most important requirement for this technology is that BTS in the network is observed by at least one LMU. Further, special software is required in MS to support E-OTD. The need for LMUs introduces significant infrastructure changes, as it requires the installation of thousands of LMUs in GSM/GPRS networks. This needs significant network planning, an assessment of the RF impact to the network, adherence to local ordinances where new sites are involved, and the expense to plan, install, test and maintain the network of LMUs. This level of intricacy complicates the operator's ability to provide roaming support for an E_OTD based location service and extends the time required to deploy network-wide location services.

E-OTD offers improved performance relative to Cell-ID, but requires the use of LMUs. This increases the cost and complexity of implementation, as described above. E-OTD also requires that a large number of data messages be exchanged to provide location information. And this information is updated constantly. This message traffic is much greater than used for A-GPS or Cell-ID, and E-OTD uses more network bandwidth than these technologies. The accuracy is affected by multi-path and signal reflections as it utilizes at least three base stations. The system is quite inaccurate in rural areas as there is lesser number of BTS [35].

3.1.2.1.2 Time of Arrival (TOA) and Time-Difference of Arrival (TDOA)

TOA works by the handset bouncing a signal back to the base station, or vice-versa. Since radio waves travel at the speed of light (c), the distance (d) between the handset and the base station can be estimated from the transmission delay. (i.e. half the time delay between transmitting and receiving the signal). This, however, only places the handset as being on a circle with a radius d, with the base station at the centre of the circle. But if the estimate were instead made from three base stations, there would be three circles that would intersect at the exact location of the handset, as shown in Fig 3.2.

TDOA is a quite similar time-based technique. It works by measuring the relative arrival time at the handset of signals transmitted from three base stations at the same time, or vice versa (by measuring the relative arrival time at three base stations transmitted by the handset). The difference of arrival time defines a hyperbola, with the

loci at the two base stations. As three base stations are used, there are three sets of time differences, which create three hyperbolic equations that define a single solution.

TDOA is sometime referred to TOA because – in most implementations – it requires less data to be exchanged over the wire connection. Precise synchronisation of the base stations is also essential for this technique to work. Should additional accuracy be required, as serving base station instructs the handset to hand-off, which causes the phone to transmit a new registration message. This message gives the base station a new set of data to make a second estimate [36].

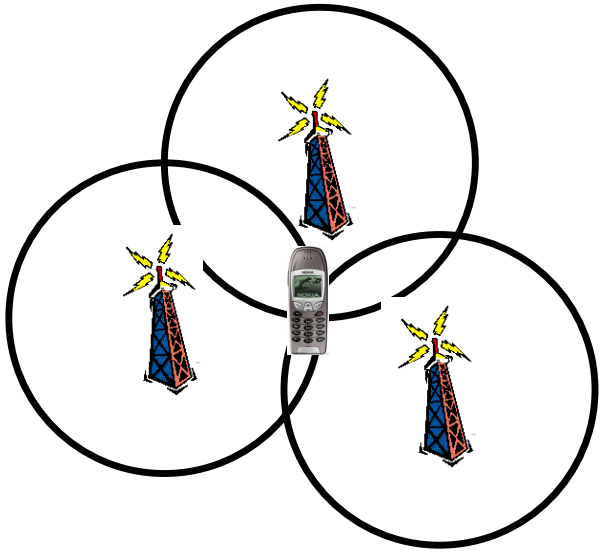

Figure 3.2: TOA Technique

3.1.2.1.3 Angle of Arrival (AOA)

AOA is based on a classic radio-direction finding technique where a highly directional antenna determines a line of bearing between a handset and a BTS. The relative angles

can then be calculated using the phase differences across the array, or by measuring the power density across the array.

Once the measurement has been made – normally from at least three base stations – the location can be calculated by simple triangulation. Unfortunately, this technique requires a line-of-sight connection between the handset and the base station, as reflected signals will provide a false line of bearing. Because GSM networks don't operate exclusively under the line-of-sight conditions, this method is often used in conjunction with another location technique [36].

3.1.2.2 Assisted Global Positioning System (A-GPS)

Like E-OTD, A-GPS is also a time–based technique in which the handset measures the arrival time of three or more signals, but in this case these are transmitted from GPS satellites as shown in Fig.3.3 below.

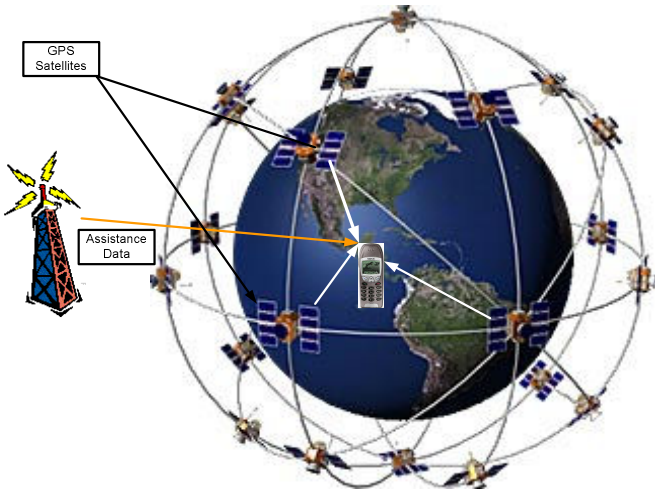

Figure 3.3: A-GPS method

In general, the information decoded by the GPS receiver is then transmitted to the handset through the radio network. This bring improvements on both the 'time to first fix' (the time it takes to obtain the first location measurement) and battery life – as the handset no longer needs to search for and decode the signals from each available satellite.

Removing the need to decode the satellite signals also enables detection and TOA estimation, which have the capability to locate a handset even under foliage, within cars, in most outside environments and many indoor environments. A-GPS also provides good vertical accuracy and velocity estimates. Signals of GPS assistance data to the handset may take 10 second, but – once received by the handset – assistance data is useful for up to four hours [36].

Currently, GPS based location information services are in commercial use - when accurate signal strength measurements from at least three Base Stations are available, geometrical (triangulation) methods are used to determine the two-dimensional (2-D) location co-ordinates of the mobile user. However, in a city or building where there is often no direct Line of Sight (LoS) between GPS satellite and the mobile terminal, this causes a severe degradation of accuracy. In such cases, location estimation using cellular network systems can offer advantages, and estimating a location using the signal from BS's becomes a highly non-linear problem [37].

3.2 *Conclusions*

This chapter has reviewed and critically evaluated the predominant location estimation techniques in use. The next chapter presents a new neural network based approach for location estimation in both simulated and real urban environments.

Chapter 4

4 New Neural Network Based Location Estimation Approach

This chapter presents a new neural network based approach to the prediction of mobile locations using signal strength measurements in simulated and real urban (metropolitan) areas. The prediction of a mobile location using propagation path loss (signal strength) is a very difficult and complex task. Several techniques have been proposed recently mostly based on linearized, geometrical and maximum likelihood methods. An alternative approach based on artificial neural networks is proposed in this chapter which offers the advantages of increased flexibility to adapt to different environments and high speed parallel processing.

4.1 *Overview of Neural Networks Employed*

Many authors have shown that neural networks provide a good way of approximating non-linear functions [2, 3]. The application of neural networks discussed in this chapter is considered as a function approximation problem consisting of a non-linear mapping of signal strength input (received at several Base Stations) onto a dual output variable representing the mobile location co-ordinates. The signal strength data is generated using COST-231 Walfisch Ikegami Non-line of Sight (NLOS) models which was reviewed in chapter 2, on account of its extensive use in practice in typical suburban and urban environments where the building heights are quasi-uniform. The designers of

the public mobile radio systems (e.g., GSM, PCS, DECT, DCS, etc.) also often use this model [10].

Next we present a brief overview of the neural network models used in this work, namely the Multi-Layered Perceptron and Generalized Regression Neural Networks.

4.1.1 Multi-layered Perceptron (MLP)

The general structure of a multi-layered perceptron (MLP), also sometimes known as the back propagation network is illustrated in Figure 4.1, with inputs x_i and outputs y_i respectively, and the network can comprise one or more hidden layers.

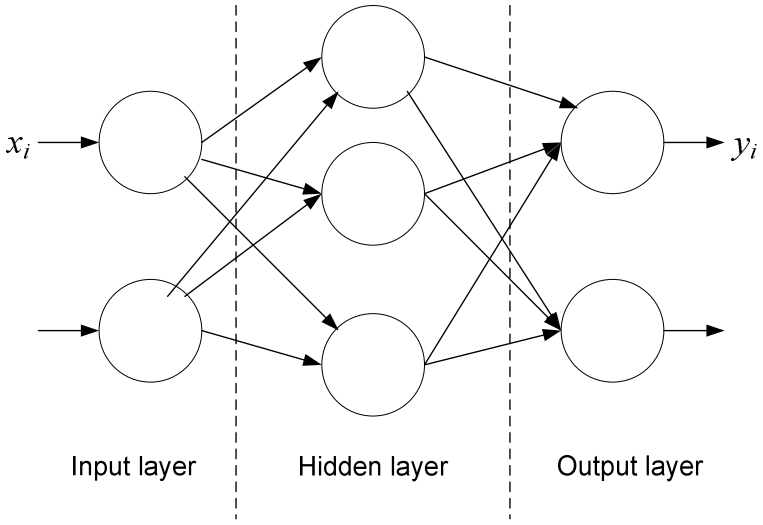

Figure 4.1: General architecture of MLP

In the MLP structure illustrated in Figure 4.1 above, the output y_i of each neuron of the *n*-th layer is defined by a derivable nonlinear function F [59]:

$$y_i = F\left(\sum_j w_{ji} y_j\right) \qquad (4.1)$$

Where F is the nonlinear activation function, w_{ji} are the weights of the connection between the neuron N_j and N_i, y_j is the output of the neuron of the $(n-1)^{th}$ layer. In our application, the neural networks are trained with the Levenberg-Marquardt algorithm, which converge faster than the back propagation algorithm with adaptive learning rates and momentum. The Levenberg-Marquardt rule for updating parameters (weights and biases) is given by [38]:

$$\Delta W = \left(J^T J + \mu I\right)^{-1} J^T e \qquad (4.2)$$

where e is an error vector, μ is a scalar parameter, W is a matrix of networks weights and J is the Jacobian matrix of the partial derivatives of the error components with respect to the weights.

4.1.2 Generalized Regression Neural Network (GRNN)

The generalized regression neural network (GRNN) [40, 41] is a feed-forward neural network based on non-linear regression theory consisting of four layers: the input layer, the pattern layer, the summation layer, and the output layer (see Figure 4.2).

While the neurons in the first three layers are fully connected, each output neurons is connected only to some processing units in the summation layer. The individual pattern units compute their activation using a radial basis function, which is typically the Gaussian kernel function. The radial basis function has a maximum of 1 when its input is 0. As the distance between the input vector and the weight vector decreases, the output increases. Thus the radial basis neuron acts as a detector which produces 1 whenever the input is identical to its weight vector.

The summation layer has two different types of processing: the summation units and a single division unit. The number of the summation units is always the same as the number of the GRNN output units. The division units only sum the weighted activation of the pattern units without using any activation function.

The training of the GRNN is quite different from the training used for the BPNN. It is completed after presentation of each input-output vector pair from the training set to the GRNN input layer only once; that is, both the centers of the radial basis functions of the pattern units and the weights in connections of the pattern units and the processing units in the summation layer are assigned simultaneously. The training of the pattern units is unsupervised, but employs a special clustering algorithm, which makes it unnecessary

to define the number of pattern units in advance. Instead, it is the radius of the clusters that needs to be specified before the training starts. The GRNN computes the predicted values "on the fly" from the training values, using the basis functions defined below [42]:

$$f(x_k) = \sum_{j=1}^{N} t_j \phi_{kj} \Big/ \sum_{j=1}^{N} \phi_{kj},\ k = 1, 2, \ldots, M. \tag{4.3}$$

In the RBFN, the computation of the predicted values is similar:

$$f(x_k) = \sum_{j=1}^{N} w_j \phi_{kj}, \quad k = 1, 2, \ldots, M \tag{4.4}$$

However, the weights are computed from the training data using the following linear equations:

$$t(\boldsymbol{x}_i) = \sum_{j=1}^{N} w_j \phi_{ij},\ i = 1, 2, \ldots, N,\ and\ \phi_{ij} = \exp\left[-\frac{\left| \boldsymbol{x}_i - \boldsymbol{x}_j \right|^2}{\sigma^2} \right] \tag{4.5}$$

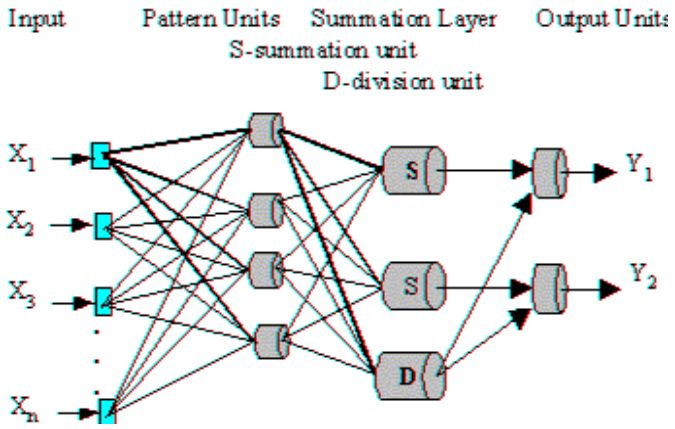

Figure 4.2: General Regression Neural Network (GRNN) [42]

4.2 *Network Architecture Simulation*

The mobile architecture used for the simulations (all carried out in MATLAB) is discussed here. For the sake of simplicity, a square cell of dimensions 3km X 4km is assumed, as shown in Figure 4.3.

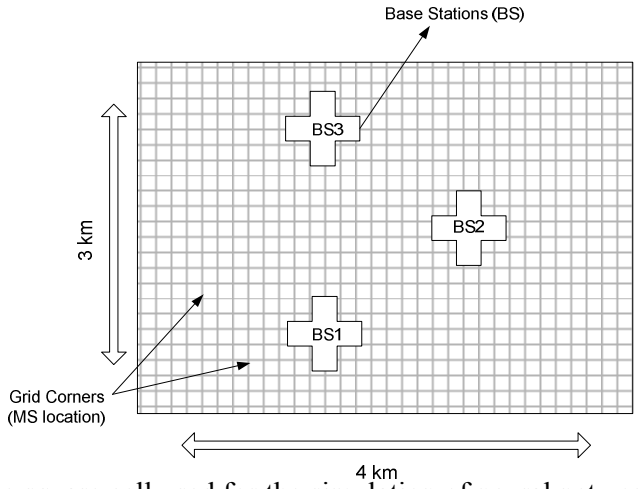

Figure 4.3: The square cell used for the simulation of neural network assisted location estimation

Three fixed BS's are used for measuring signal strengths. The coverage area is divided into grids of different dimensions (determined by the grid size, which was varied from 0.1km to 0.9km) for training purposes. The idea is to place the mobile in each of these grid intersections and transmit the signal. All the three BS's measure the received signal strengths from each position of the mobile [1]. The neural net is trained on the generated data using the corresponding mobile location co-ordinates as its target outputs. The origin of coordinates is taken at the left bottom corner and all measurements are taken relative to it. The trained neural network's generalization capability is assessed by testing on data generated with a different grid size (varying from 0.1km to 0.3km) to that used for training.

4.3 *Performance Evaluation Metric*

Following [52], we use the mean distance error metric to evaluate the accuracies of our location algorithms. Mean distance error represents average Euclidean distance between the estimate ($\hat{x}$, $\hat{y}$) and the true location (x, y), i.e.

$$d = \sqrt{(x - \hat{x})^2 + (y - \hat{y})^2} \qquad (4.6).$$

4.4 *Simulation Results & Discussion*

We now investigate the effect of the grid size and the number of base stations on the location accuracy with the various location predictors.

4.4.1 Simulation Results using Simulated Data

The COST231 model represented by equations 2.16 to 2.29 was implemented to generate the required training and test data. The number of base stations was set to 2 and 3 and the training grid size was fixed to 0.3km (i.e. the coverage area was divided into grid of dimensions 0.3km x 0.3km). The grid size for generating the test data was set to 0.1km.

Three base stations were used to generate the training data, and the configurations of the various location techniques to be compared (namely, the MLP, GRNN and Linear Adaptive filters) were determined experimentally as described below and their performance evaluated using the MDE metric.

4.4.1.1 MLP based location estimation

For the situation described in Figure 4.3, the training set consisted of 154 samples of signal strength measurements received at the three fixed BSs and the corresponding mobile location co-ordinates. A two-hidden layered (3-4-8-2) MLP comprising 3 inputs, 2 hidden layers of 4 and 8 nodes, and 2 outputs, was trained using the Levenberg-Marquardt back propagation algorithm [4], and the mean distance error (MDE) was calculated to equal 0.0517km after 145 epochs, with the result that the net maps any measurement of the training set perfectly to the location of MS for that set. For testing the trained neural network's generalised capability, points other than the training set were generated within the same (3km x 4km) coverage area by dividing the coverage area into smaller grids of dimensions 0.1km X 0.1km (rather than the 0.3km x 0.3km grids used to generate the training data). Note that use of different grid sizes is a simple way of generating the simulated training and test sets, and other more conventional ways could also be explored and compared, such as, by using parts of the same data (generated at a fixed grid size) for training and test purposes. An approach similar to this has been adopted for the case of real signal strength data used in section 4.4.2. Comparison of the various approaches reported in literature [38] for selection of training and test sets is proposed for future work in Chapter 6.

Sample test results for the MLP location predictor (for the x and y co-ordinates) are shown in Figures 4.4 & 4.5 respectively, for which the mobile was assumed to be at 1271 different points on the test grid. These points on the grid were obtained by varying the y position of the mobile on the grid for each fixed x position. Each increment of the x and y location coordinate was set equal to the grid size (0.1km for the case of test data

generation) and the maximum value of the x and y co-ordinates were set to the associated coverage area dimensions, namely 4km for the x co-ordinates and 3km for the y co-ordinates respectively. As a result, the x and y co-ordinate values can be seen to have different characteristics, namely the x co-ordinates take an 'incrementing step' shaped form (as shown in Figure 4.4) whereas the y co-ordinates take a 'ramp-like' form (as shown in Figure 4.5).

Test Data				
BS1	**BS2**	**BS3**	**X Coordinates**	**Y Coordinates**
133.09	141.47	136.57	0	0.8
133.13	141.37	136.18	0	0.9
133.21	141.29	135.81	0	1
133.33	141.22	135.44	0	1.1
133.49	141.17	135.09	0	1.2
133.69	141.13	134.76	0	1.3
133.91	141.11	134.46	0	1.4
134.17	141.1	134.17	0	1.5
134.46	141.11	133.91	0	1.6
134.76	141.13	133.69	0	1.7
135.09	141.17	133.49	0	1.8
135.44	141.22	133.33	0	1.9
135.81	141.29	133.21	0	2
136.18	141.37	133.13	0	2.1
136.57	141.47	133.09	0	2.2
136.97	141.58	133.09	0	2.3
137.37	141.71	133.13	0	2.4
137.78	141.84	133.21	0	2.5
138.19	141.99	133.33	0	2.6
138.6	142.15	133.49	0	2.7
139.01	142.32	133.69	0	2.8
139.42	142.5	133.91	0	2.9
139.83	142.69	134.17	0	3
133.43	142.27	139.47	0.1	0
133.15	142.07	139.04	0.1	0.1
132.9	141.88	138.61	0.1	0.2

Table: 4.1: Sample simulated test data

Figures 4.6 and 4.7 show a selected part of the target (test) versus MLP predicted X and Y location coordinates. Finally, the estimation (prediction) errors for the X and Y co-ordinates are shown in figures 4.8 and 4.9 from which it can be seen that the maximum prediction error in the X and Y location co-ordinates are around 0.005km and 0.007km respectively. Note that the MLP predictions on the test data can, of course, be further improved by training the net on a larger set of readings (using a smaller grid than 0.3km x 0.3km).

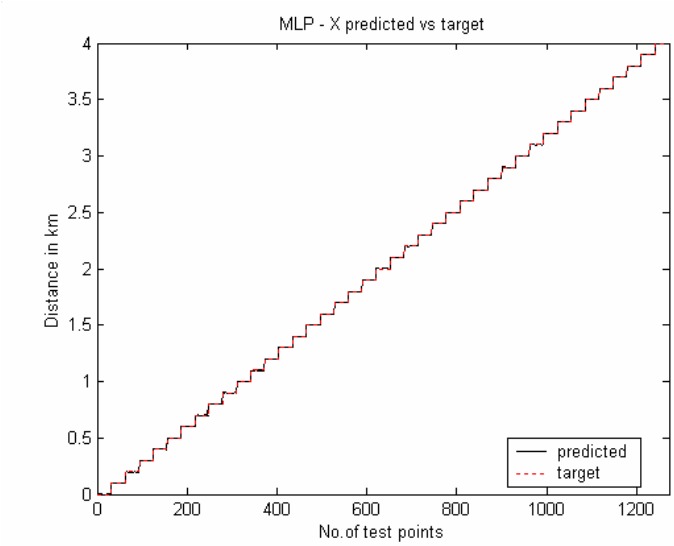

Figure 4.4: X-location co-ordinates for MLP with 3 BS's using simulated data - predicted vs target test data)

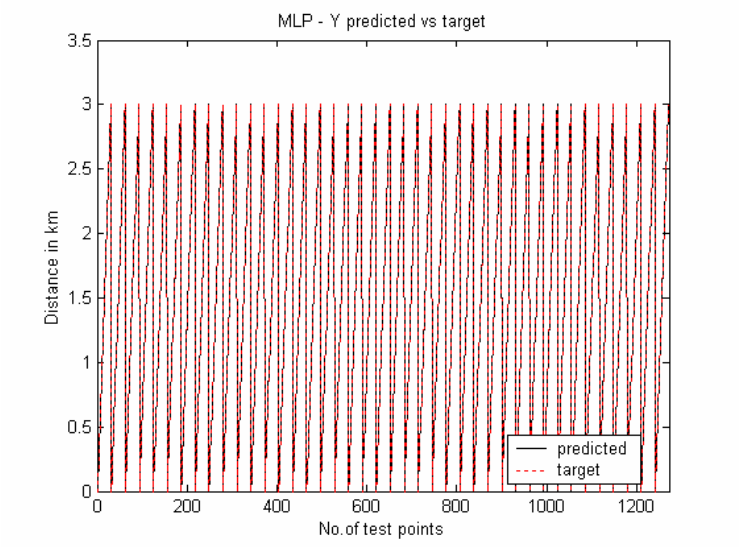

Figure 4.5: Y-location co-ordinates for MLP with 3 BS's using simulated data - predicted vs target test data)

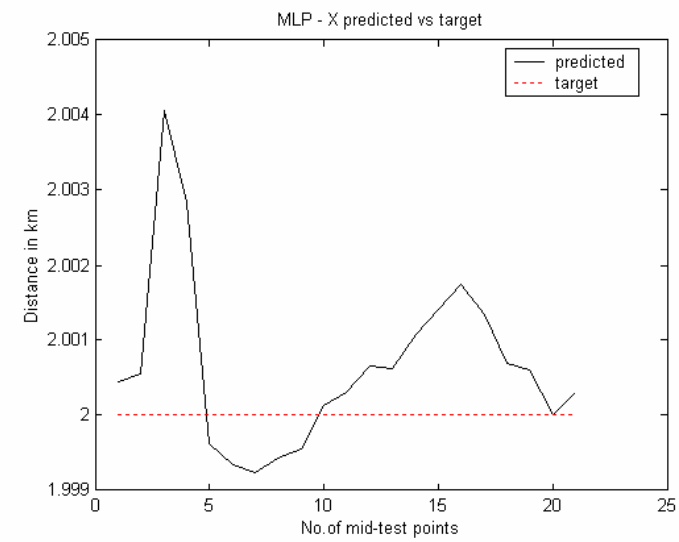

Figure 4.6: Part sample X-location co-ordinates for MLP network with 3 BS's using simulated data - predicted vs target test data

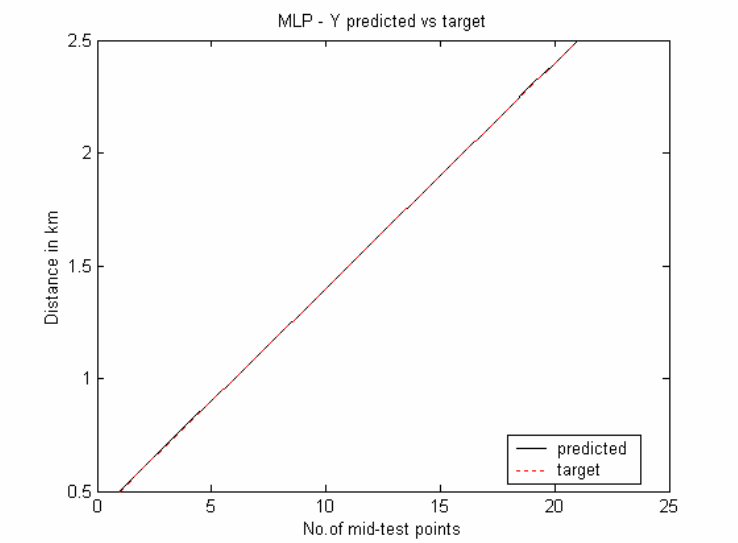

Figure 4.7: Part sample Y-location co-ordinates for MLP network with 3 BS's using simulated data - predicted vs target test data

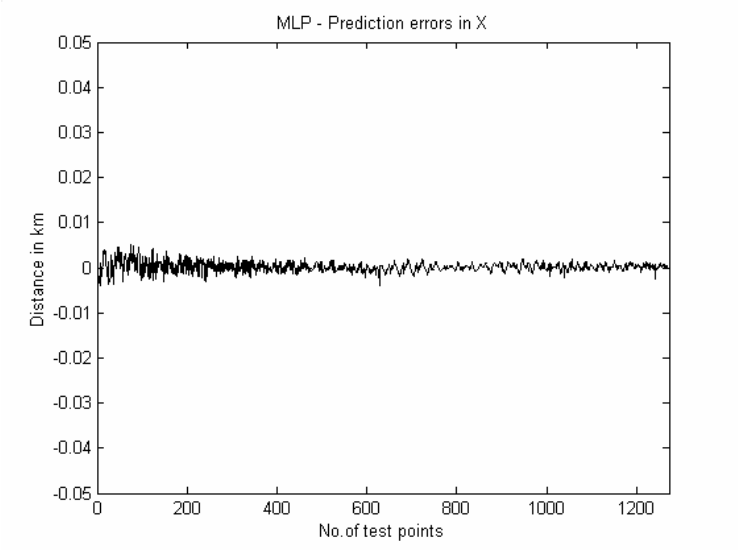

Figure 4.8: Estimation error in X co-ordinates for MLP Predictor using simulated data and 3 Base stations (Note Y-axis scale: ±0.05km)

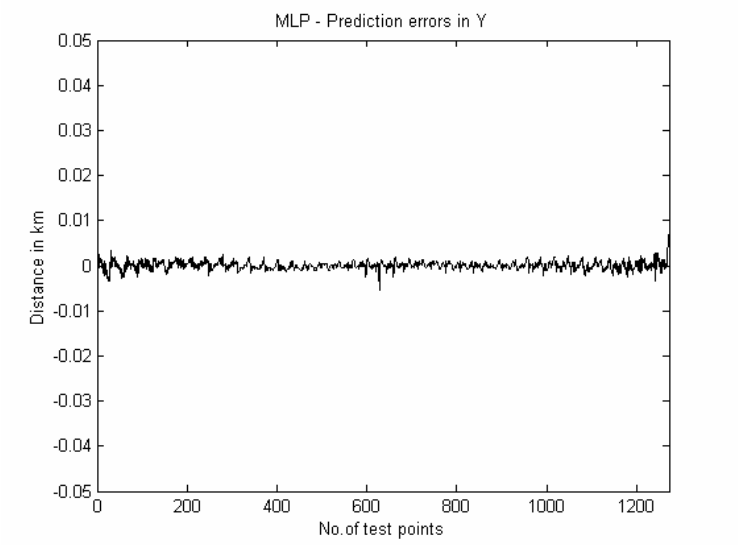

Figure 4.9: Estimation error in Y co-ordinates for MLP predictor using simulated data and three base stations (Note Y-axis scale: ±0.05km)

4.4.1.2 GRNN based location estimation

Another neural network namely the Generalised Regression Neural Network (GRNN) was used for the situation described in Figure 4.3 above for performance comparison. As mentioned earlier, GRNNs are a kind of radial basis networks that are often used for function approximation [41].

As per the case for the MLP above, the training set for the GRNN consisted of 154 samples of signal strength measurements received at the three fixed BSs (generated with a grid size of 0.3km x 0.3km) and the corresponding mobile location co-ordinates.

For testing the trained neural network's generalised capability, points were again generated within the same (3km x 4km) coverage area by dividing the coverage area into grids of dimensions 0.1km X 0.1km. The GRNN location estimation (prediction)

errors for the X and Y co-ordinates are shown in Figures 4.10 and 4.11, from which it can be seen that the maximum prediction error in X- and Y-location co-ordinates are around 0.4km and 0.266km respectively.

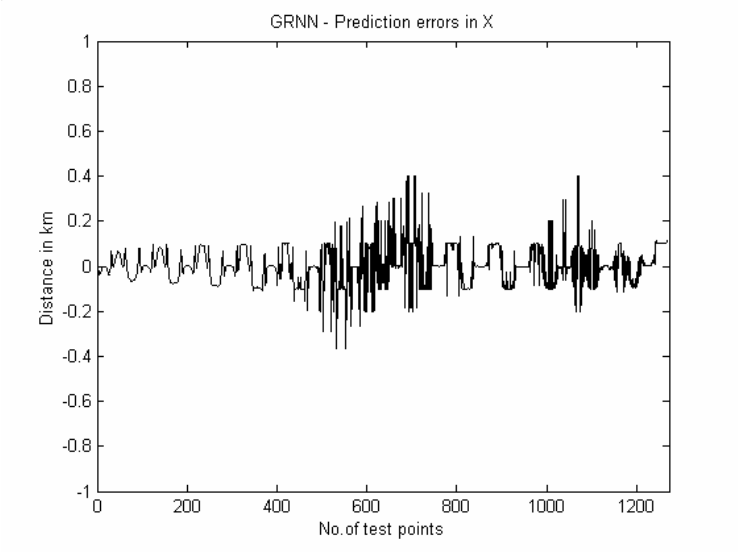

Figure 4.10: Estimation error in X co-ordinates for GRNN predictor using simulated data and three base stations (Y-axis range: ±1km)

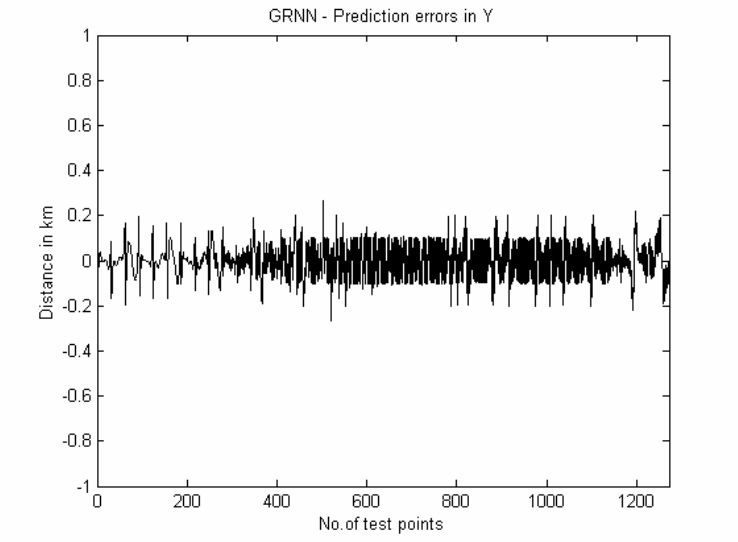

Figure 4.11: Estimation error in Y co-ordinates for GRNN predictor using simulated data and three base stations (Y-axis scale: ±1km)

4.4.1.3 Linear Adaptive Filter based location estimation

For comparison purposes, a linear adaptive filter, employing a Finite Impulse Response (FIR) structure and least squares based adaptation [38] with four inputs (including one bias input), was also trained and tested on the same data sets as the MLP and GRNNs.

The location estimation (prediction) errors for the X and Y co-ordinates (for the linear predictor) are shown in Figures 4.12 & 4.13 respectively, from which it can be seen that the maximum prediction error in X- and Y-location co-ordinates are around 2km and 1.6km respectively, which are both clearly very high for the 4km x 3km grid area.. It is interesting to note the periodic pattern in the estimation errors for both the X and Y co-ordinates which are similar to the shape of the original X and Y co-ordinates (shown in Figure 4.4 and 4.5 respectively). This finding shows the inability of the linear predictor to learn the non-linear mapping from the of signal strength input onto the dual location co-ordinates.

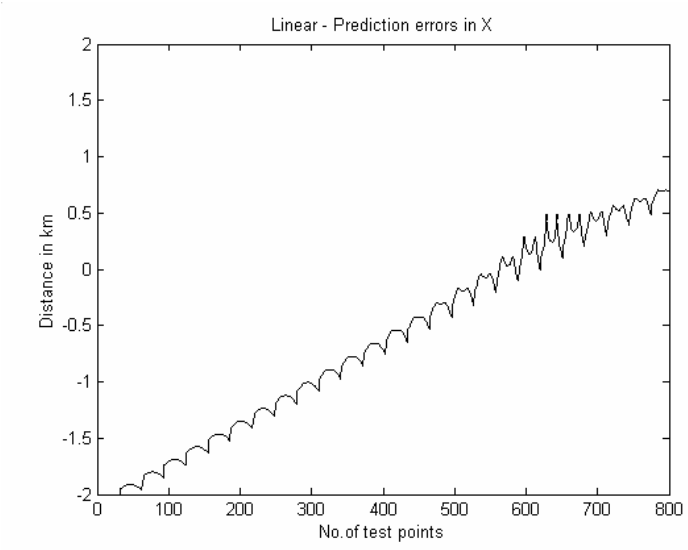

Figure 4.12: Estimation error in X co-ordinates for Linear adaptive filter predictor using simulated data and three base stations (Note Y-axis scale: ±2km)

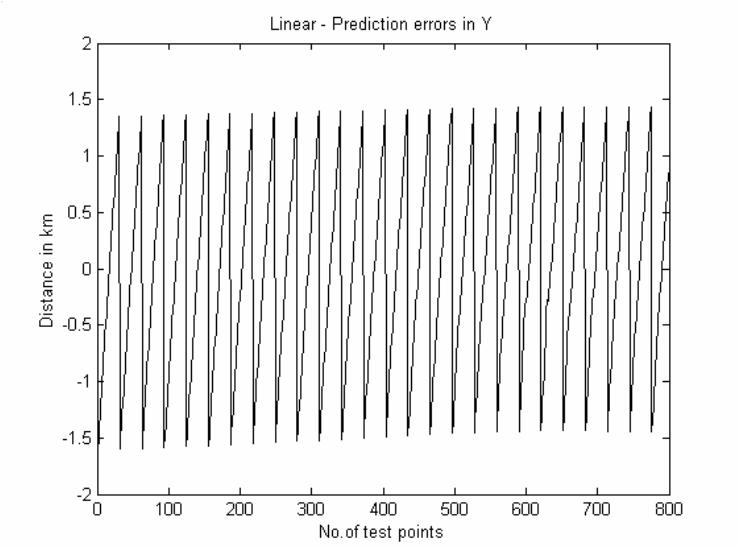

Figure 4.13: Estimation error in Y co-ordinates for Linear adaptive filter predictor using simulated data and three base stations (Note Y-axis scale: ±2km)

Finally, Table 4.2 summarizes and compares the performance of the MLP, GRNN and a conventional linear adaptive filter in terms of the Mean Distance Error (MDE). As can be seen from Table 4.2, the MLP based location predictor gives the best MDE performance on the test set followed by the GRNN and the adaptive linear predictor, which as expected is found to exhibit the worst MDE performance on account of its inherent inability to approximate the non-linear mapping of signal strength input (received at the three Base Stations) onto the dual output variable representing the mobile location co-ordinates.

Location Predictor Used	Training Set size (grid size=0.3km^2)	Test Set Size (grid size=0.1km^2)	Mean Distance Error (km)	Maximum Error X (km)	Maximum Error Y (km)	No. of BS
MLP	154	1271	0.0517	0.0051	0.0071	3
GRNN	154	1271	4.2218	0.4000	0.2666	3
Linear	154	1271	52.3923	2.0653	1.6074	3

Table: 4.2: MDE Performance comparison of Location Predictors with Signal Strength Measurements using Three Base Stations

4.4.1.4 Effect of grid size on Location Accuracy (for simulated data)

The effect of varying the grid size for the COST231 propagation model on the location accuracy was experimentally investigated. For this purpose, the test grid size was fixed to 0.1kmx0.1km (resulting in 1271 test data points) whereas the training grid size was varied between 0.1kmx0.1km (resulting in 1271 training data points) to 0.7kmx0.7km (resulting in 30 training data points). The MDE results of the MLP location predictor are shown in Table 4.3 and plotted in Figure 4.14. It can be seen from both Table 4.3 and Figure 4.14 that, as expected, the training MDE performance of the location predictor improves with the increasing size of training set (generated using small grid sizes). However, in a real environment, a trade-off would have to be determined between the grid size (used for generating the training set) and the desired accuracy of location estimation on the unseen test set.

Location Predictor Used	Training Set Grid Size (km2)	Training Set size	Test Set Size	Mean Distance Error (km)	No. of Base Stations
MLP	0.1	1271	1271	0.0503	3
	0.3	154	1271	0.0528	3
	0.5	63	1271	0.1567	3
	0.6	42	1271	2.8607	3
	0.7	30	1271	3.6073	3

Table: 4.3: MDE Performance vs Grid Size

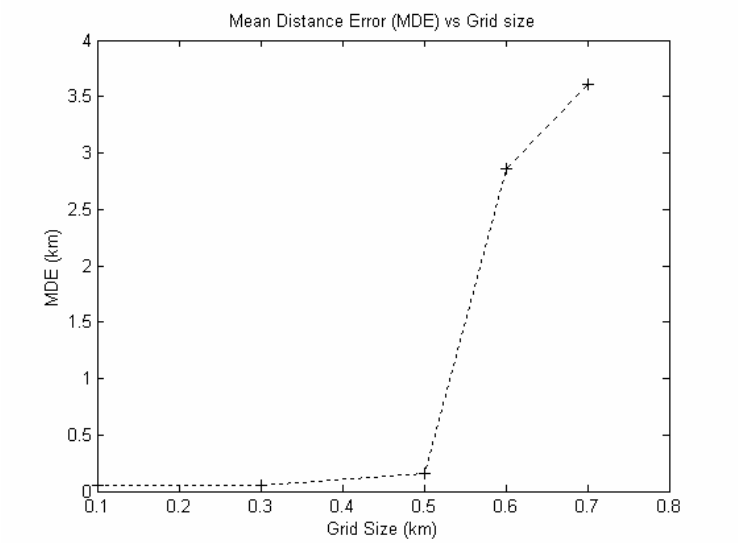

Figure 4.14: Mean Distance Error vs Grid Size

4.4.2 Simulation results using real data

Limited real signal-strength data was obtained for evaluation purposes from a UK telecommunications company, which was measured in a small English town, Chippenham. The measurements were obtained from three base stations. Additional information on the real data was not available.

4.4.2.1 Case I: Performance comparison of Location Predictors using Real Data from 3 BSs

The performance of the linear and two neural network predictors, namely the MLP and GRNN models, was evaluated on the 772 sample real data set which, due to its very limited size, was arbitrarily partitioned into a 501 sample training set and a 271 sized test set. The structure and parameters of the neural and the linear predictors were obtained experimentally using a trial and error approach. The best MLP predictor's structure comprised three inputs (corresponding to the three BS signal strength measurements), two hidden layers of 8 and 16 (sigmoidal) nodes respectively, and two

outputs (representing the dual output co-ordinates). On the other hand, the best GRNN predictor also comprised three inputs, two outputs and two hidden layers, but with the first hidden layer consisting of 501 Gaussian RBF neurons corresponding to the number of input/target vectors (and with a spread of 1.2 which was experimentally selected to provide a smooth fitting of the data) and the second layer comprising 501 linear (summation) neurons. Lastly, the best linear (least squares based) predictor comprised 4 weights (co-efficients) estimated using the least squares method. The MDE performance measures obtained by the three location predictors are illustrated in Table 4.4.

As can be seen from the Table 4.4, the MLP predictor gives the best MDE performance (with the lowest MDE of 0.0482km, and maximum X and Y co-ordinate prediction errors of 0.005km and 0.0069km respectively) closely followed by the GRNN (with an MDE of 0.0526km) and the linear adaptive predictor which gives the worst performance as expected (with an MDE of 223km). For illustrative purposes, the results for the MLP predictor (X and Y location co-ordinate predictions) are also shown in Figures 4.15 and 4.16 respectively, along with the corresponding prediction errors which are illustrated in Figures 4.17 and 4.18 respectively.

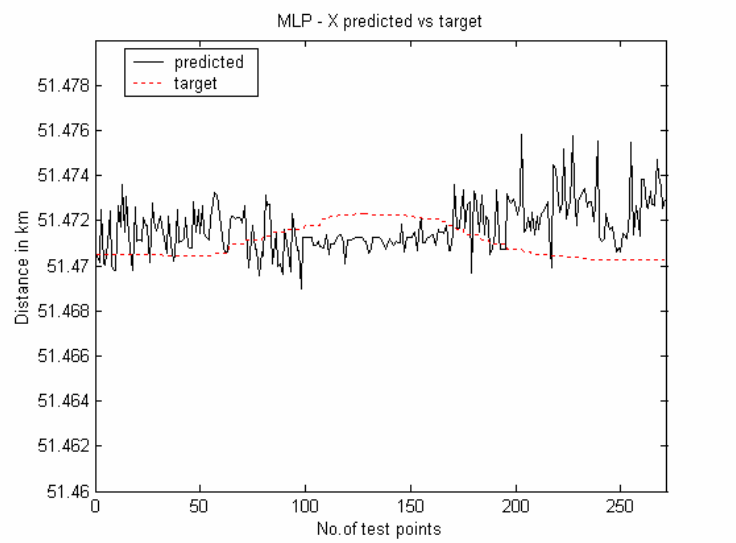

Figure 4.15: X-location co-ordinates (MLP predicted vs target test data)

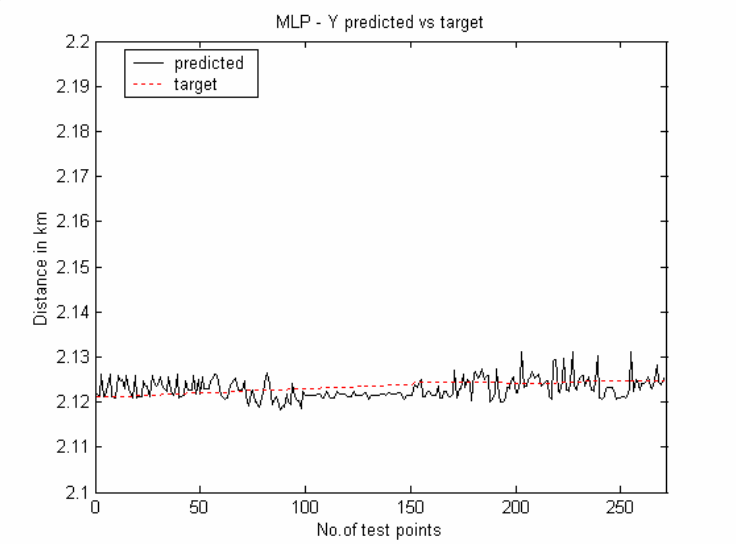

Figure 4.16: Y-location co-ordinates (MLP predicted vs target test data)

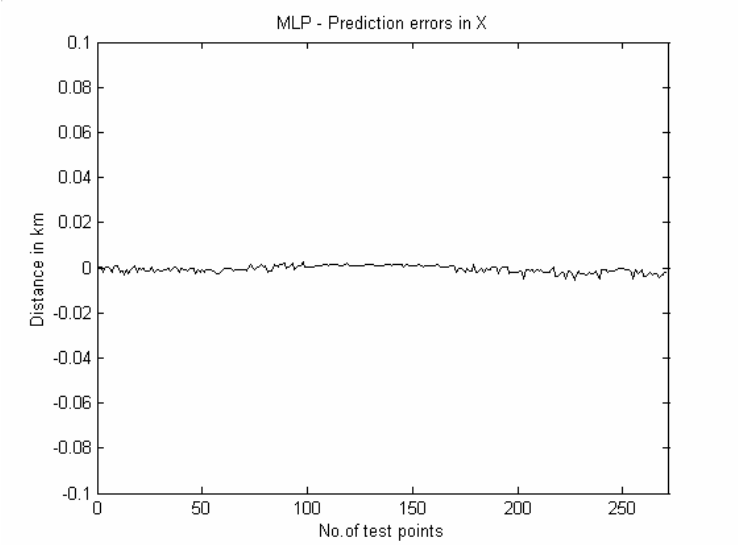

Figure 4.17: Estimation error in X co-ordinates for the MLP location predictor

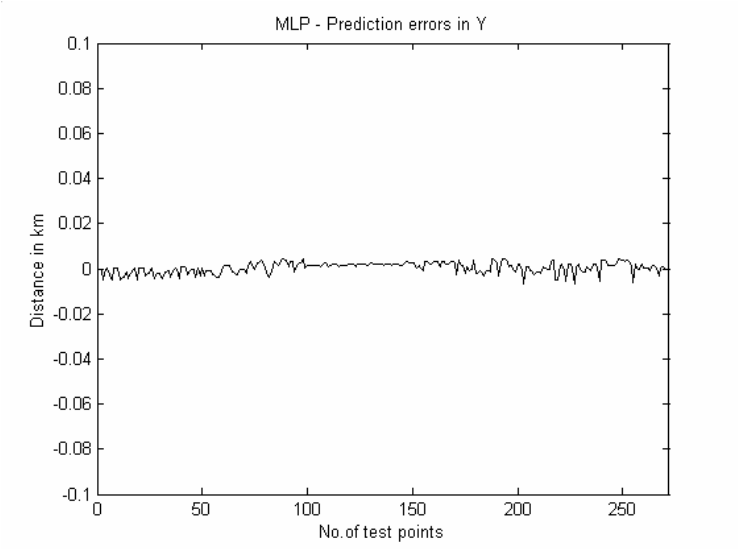

Figure 4.18: Estimation error in Y co-ordinates for the MLP location predictor

Location Predictor Used	Training Set size (grid size=0.3km^2)	Test Set Size (grid size=0.1km^2)	Mean Distance Error (km)	Maximum Error X (km)	Maximum Error Y (km)	No. of BS
MLP	501	271	0.0482	0.0054	0.0069	3
GRNN	501	271	0.0526	0.0049	0.0066	3
Linear	501	271	223.1791	33.8377	1.3953	3

Table: 4.4: MDE Performance comparison of Location Predictors with Signal Strength Measurements using Three BSs

4.4.2.2 Case II: Performance comparison of Location Predictors using Real Data from two BSs

Next, the performance of the two neural predictors was compared for the case of data measurements taken from just two BSs. The MDE performance measures are shown in Table 4.5, from which it can be seen that both the neural location predictors are still capable of providing accurate location estimates in spite of the very limited information available. For this case, the GRNN predictor can be seen to be slightly more effective compared to the MLP predictor in providing accurate locations estimates in spite of having been trained on measurements from only 2 BSs, yielding a MDE of 0.0430km (with maximum X and Y co-ordinate prediction errors of 0.005km and 0.0069km respectively) compared to the MLP's MDE of 0.0044 (with maximum X and Y co-ordinate prediction errors of 0.0063km and 0.0058km respectively). However, since this study has only involved very limited (available) real data, additional experiments will need to be conducted in order to draw more general conclusions about the comparative performance evaluation of the two neural predictors.

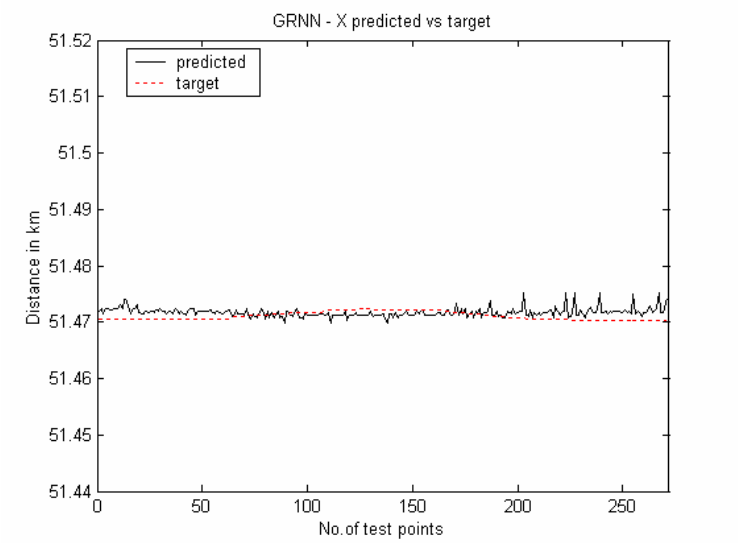

Figure 4.19: X-location co-ordinates for GRNN predictor: predicted vs target test data for 2 BSs

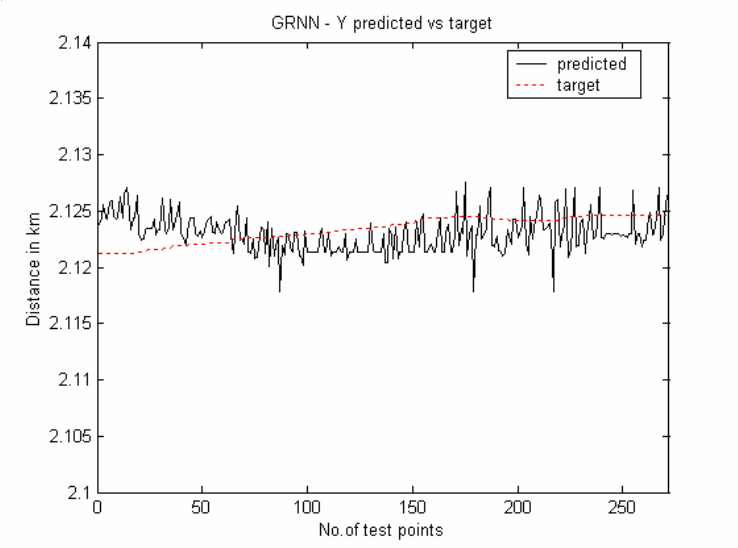

Figure 4.20: Y-location co-ordinates for GRNN predictor: predicted vs target test data for 2 BSs

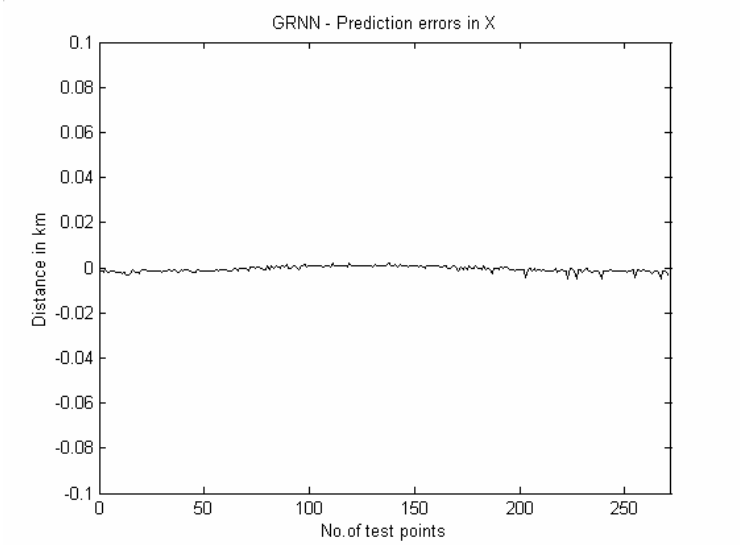

Figure 4.21: Estimation error in X co-ordinates for the GRNN location predictor

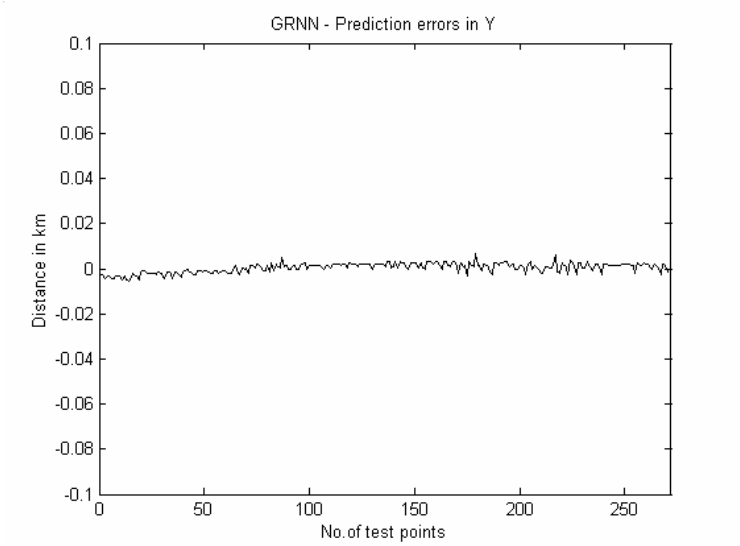

Figure 4.22: Estimation error in Y co-ordinates for the GRNN location predictor

Location Predictor Used	Training Set size (grid size=0.3km^2)	Test Set Size (grid size=0.1km^2)	Mean Distance Error (km)	Maximum Error X (km)	Maximum Error Y (km)	No. of BS
MLP	500	270	0.0444	0.0063	0.0058	2
GRNN	500	270	0.0430	0.0049	0.0066	2

Table: 4.5: MDE Performance comparison of Location Predictors with Signal Strength Measurements using Two BSs

4.5 Discussion & Conclusions:

This chapter has presented new MLP and GRNN neural network based location predictors which have been shown to be capable of performing effective approximation of the non-linear mapping of signal strength input (received at the two or more Base Stations) onto the dual output variable representing the mobile location co-ordinates. The MDE performance of the various location predictors was investigated for the case of a simulated mobile architecture employing the COST-231 NLOS propagation model. It was found that the MLP location predictor was more effective than the RBF based GRNN and linear predictors. Next, the performance of the neural predictors was evaluated using very limited real data provided by a UK telecommunications company (for a small UK town), and both the neural predictors were found to produce impressive location predictions for the case of data from three BSs. Following this, additional simulation results were used to demonstrate that both the neural predictors are capable of providing almost equally accurate location estimates even in the case of more limited real data from just two BSs. This is a very interesting finding which needs further investigation (using more extensive real data from a range of urban and indoor environments).

Note that the parameters (number of hidden layers, neurons, learning rates, RBF centres, spreads etc.) were all determined experimentally using a trial and error

approach and are thought to be reasonable but these could be further optimised. In conclusion, it can be argued that the MLP predictor can perform better than the GRNN in terms of the MDE performance measure. As mentioned earlier, a reduction in the number of BSs from three to two was found to have minimal detrimental effect on the MDE performance measure of both the neural location predictors. On the contrary, for the case of the conventional tri-lateration technique, an accurate and unique determination of the relative location of a point on a 2D plane requires at least 3 reference points.

The next chapter reviews the co-channel interference suppression problem in cellular networks and compares the performance of selected neural network based equalizers for overcoming co-channel interference in co-channel systems.

Chapter 5

5 Neural Networks for Co-Channel Interference Suppression in Cellular Networks

In this chapter, the problem of adaptive equalization of digital communication channels in the presence of co-channel interference is briefly reviewed. An overview of conventional approaches to the problem including the use of neural networks is presented and selected neural networks are then applied to the problem of adaptive equalization in the presence of Inter-Symbol Interference (ISI), Additive White Gaussian Noise (AWGN), and Co-Channel Interference (CCI). The neural network based equalizers are shown to work without any prior knowledge of the interfering signals or the transmission and co-channel orders. Finally, a realistic severe amplitude distorted co-channel system is used as a case study to illustrate the superior Bit Error Rate (BER) performance of the functional-link neural network based Decision Feedback Equalizer compared to other conventional linear and non-linear neural network equalizers.

5.1 Introduction

Adaptive equalization is known to be an important technique for combating distortion and Inter-Symbol Interference (ISI) in communication channels. However, many communication systems are also impaired by what is known as co-channel interference (CCI). Many digital communications systems such as digital cellular radio (DCR)

systems encounter CCI, adjacent channel interference (ACI), ISI and AWGN. The CCI is caused due to frequency reuse and the frequency spacing in different cells contributes to the ACI. While these effects affect the DCR in particular, the effects of ISI due to narrow-band channel characteristics affect all digital communication systems in general. Frequency reuse is referred to the employment of radio channels on the same carrier frequency to cover different areas or cells situated sufficiently apart from one other, and allow cellular radio systems to handle far more simultaneous calls than the total number of allocated channel frequencies. Signals for co-channel cells (i.e. cells of the same channel frequency) will however interfere with each other thus requiring the use of adaptive equalizers in these communications systems for reliable data transmission. In DCR applications, CCI primarily limits the performance of the equalizers. Therefore, simple and effective interference suppression techniques, in the form of adaptive equalizers, are required to mitigate the interference for a high-quality signal reception.

Two basic categories of adaptive equalizers exist, namely the sequence estimation and symbol decision equalizers. The optimal sequence estimation equalizer is the Maximum Likelihood sequence estimator (MLSE) which provides the best attainable performance in combating channel ISI and Additive White Gaussian Noise (AWGN) at the expense of very high computational complexity and deferring decisions. The MLSE is however much less effective in dealing with Co-Channel Interference. It can best treat the unknown interfering signal as an additional colored noise since it is very difficult to derive the likelihood function for the non-Gaussian interfering signals to enable them to be explicitly distinguishable from the Gaussian noise [53, 62-63, 68].

Most of the equalization applications today employ equalizers that operate symbol-by-symbol. Symbol decision equalizers can be further qualified into two categories namely, the direct-modelling equalizers in which the channel model is identified explicitly, and the indirect-modelling equalizers which recover the transmitted symbols by directly filtering the channel observations, usually using the Linear Transversal Equalizer (also known as the Finite Impulse Response filter), without estimating a channel model explicitly. The indirect-modelling approach is by far most widely used and it is considered in the present study in the context of CCI. The current work primarily involves a review of the application of neural network based equalizers to the problem of combating co-channel interference, without a priori knowledge of the channel or interfering co-channel orders.

This chapter is organized as follow**:** In section 2, the discrete time model of the digital communication system is presented. Simulation results are presented in section 3, where selected neural network based equalizers are applied to a realistic co-channel system and their BER performance characteristics compared. Finally, section 4 presents some concluding remarks.

5.2 System Model

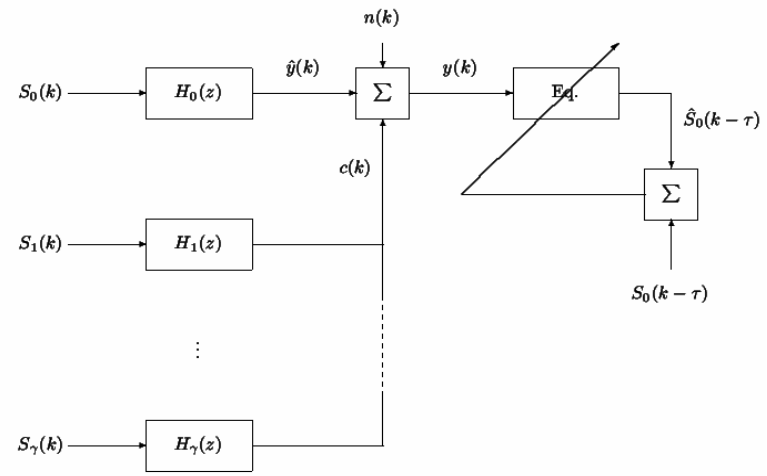

Figure 5.1: Discrete time model of the DCR system affected by CCI, ISI and AWGN.

Following [53] and [63], the discrete time model of the data transmission system considered in this work is shown in Figure 5.1. In this model, $H_0(z)$ is the dispersive channel transfer function and $H_1(z)$ . . . $H_\gamma(z)$ represent the interfering co-channels. All channels are modelled by Finite Impulse Response (FIR) filters:

$$H_i(z) = \sum_{j=0}^{li} h_{ij} z^{-j} \qquad i = 0, 1, \ldots, \gamma \qquad (5.1)$$

In Figure 5.1, $s_0(k)$ represent the transmitted data (which is known during the equalizer Training phase and $s_i(k)$, i = 1, . . .γ , are unknown interfering data sequences. All $s_i(k)$, i = 0, . . . ,γ are assumed to be equi-probable and bipolar independent identically distributed (*iid*) and the output from the co-channels $c(k)$ are corrupted by Additive White Gaussian Noise (AWGN) $n(k)$ of zero mean and variance σ_n^2.

All $s_i(k)$, $i = 0, 1, \ldots \gamma$, are assumed to be uncorrelated with $n(k)$. The overall channel observation can thus be written as:

$$y(k) = \hat{y}(k) + c(k) + n(k) \qquad (5.2)$$

where

$$\hat{y}(k) = \sum_{j=0}^{l0} h_{0j}\, s_0(k-j) \qquad (5.3)$$

where l_0 is order of the distorting channel; and

$$c(k) = \sum_{i=1}^{\gamma} \sum_{j=0}^{li} h_{ij}\, s_i(k-j) \qquad (5.4)$$

where l_i , $i = 1, \ldots \gamma$ is the order of the i - th interfering co-channel. If $E\{\hat{y}^2(k)\} = \sigma_s^2$ (where $E\{.\}$ is the expectation operator) and $E\{c^2(k)\} = \sigma_c^2$; then the following expressions can be defined:

The Signal to Noise Ratio (SNR) given by:

$$\text{SNR} = \sigma_s^2 / \sigma_n^2 \qquad (5.4)$$

The Signal to Interference Ratio (SIR) defined as:

$$\text{SIR} = \sigma_s^2 / \sigma_c^2 \qquad (5.6)$$

And finally the Signal to Interference to Noise Ratio (SINR) given by:

$$\text{SINR} = \sigma_s^2 / (\sigma_n^2 + \sigma_c^2) \qquad (5.7)$$

The task of any indirect-modelling equalizer is:

Given the overall channel observation $y(k)$, estimate the transmitted data $s_0(k)$. The symbol decision equalizer at any sample instant k processes the n most recent channel

observations, and makes a decision $\hat{s}_0(k-\tau)$ regarding the symbol transmitted at $k - \tau$, where integer n and τ are referred to as the equalizer order and delay respectively.

For decision Feedback structures, a Feedback order m is also added. Thus, $s_0(k-\tau)$ is estimated from the n most recent channel observations, and the m past decisions of the equalizer ($\hat{s}_0(k-\tau-p)$ for $p = 1,\ldots,m$). During the training period of most adaptive equalization systems (including DCR systems), the reference desired signal $s_0(k-\tau)$ which is to be re-constructed, is available, whereas the other interfering signals $s_i(k)$, $i = 1, \ldots \gamma$, are not known.

5.3 Review of Existing Equalizers

For equalization of channels in the presence of ISI, AWGN and co-channel interference, the following main developments have been reported.

Wales [60] presented a reduced complexity receiver structure for improving the tolerance of a receiver to the presence of like modulated co-channel interference. Performance improvements were demonstrated over a conventional receiver of static channels using an analytical technique, and for Rayleigh fading channels using Monte Carlo simulation techniques. However, for Rayleigh fading channels, the performance of the receiver structure was seen to degrade at high signal to interference ratios.

In [54] an equalizer structure for combating co-channel interference was described that relied upon the stronger of the wanted and interfering signals to capture a conventional

BPSK demodulator. The detected signal was then re-modulated and cancelled from the received signal to allow the detection of the weaker signal. This approach has a low complexity but performance improvements are strictly limited to the situations where the interfering signal level exceed that of the wanted signal and the technique has yet to be extended to time disperse channels.

In [50] Giridhar, Shynk and Gooch presented a non-linear co-channel demodulation techniques based on the MLSE and the Maximum Aposteriori Probability (MAP) (also known as the Bayesian transerval equalizer (TE)) symbol detection for joint recovery of both the desired and the interfering signals. However the algorithms are computationally expensive and assume perfect priori knowledge of both the primary and interfering channels. Also they provide optimal performance only for the case of comparable energies of the desired and interfering signals.

In [48] Chen and Mulgrew employed a non-linear adaptive equalizer based on the Radial Basis function (RBF) neural network to overcome co-channel interference. A complex two stage learning strategy was employed to model the effects of the channel ISI and co-channel interference and thus provide the optimal Bayesian transversal TE solution. Performance improvements were reported over the LTE for moderate to high signal to interference ratios. However, even for small orders of the primary and interfering channels, computing the optimal equalizer performance using the feedforward RBF is extremely costly and impractical as a prohibitively large number of centres are needed to present an equal number of the noise-free observation states.

Determination of the number of noise free observation states (which set the required number of RBF centres for optimal performance) also requires apriori knowledge of the orders of both the distorting channel and the unknown interfering co-channels.

Chen et al. [62] derived a new optimal Bayesian decision feedback equaliser (DFE) which incorporated co-channel interference compensation. The authors showed how decision feedback can be utilized to improve equalizer performance as well as to reduce computational complexity. The relationship between the Bayesian solution and the radial basis function (RBF) network was emphasized and two adaptive schemes were described for implementing the Bayesian DFE using the RBF network. By exploiting the structure of co-channel interfering signals, the Bayesian DFE was able to distinguish an interfering signal from white noise and utilised this information to improve performance. Adaptive implementation of the Bayesian DFE included identifying the channel model using the least mean square algorithm and estimating the co-channel states by means of an unsupervised clustering scheme. Simulation involving a binary signal constellation was used to compare both the theoretical and adaptive performance of the Bayesian DFE with those of the maximum likelihood sequence estimator. The results obtained indicated that, in the presence of severe co-channel interference, the Bayesian decision DFE employing the proposed simple scheme to compensate co-channel interference can outperform maximum likelihood sequence estimator that only treats co-channel interference as an additional coloured noise.

Patra and Mulgrew [63][70] proposed a fuzzy logic based implementation of the optimal Bayesian DFE solution and showed that the fuzzy implemented equaliser is able to provide performance close to the optimal equaliser with a reasonable reduction in computational complexity. However, like the RBF, the fuzzy implementations of the Bayesian DFE were also found to exhibit a significantly increased computational requirement for the case of large equalizer orders.

In [59], new Functional-link neural network based TE and DFE structures were developed and shown to approximate the optimal Bayesian TE and Bayesian DFE performance with a lower computational requirement compared to the RBF, MLP [45] and volterra (polynomial) neural network [46] based equalizers for the case of small equalizer orders.

Several other reduced complexity indirect modelling TE and DFE structures have been proposed to approximate the optimal Bayesian TE & DFE solutions, including more recently, the Support Vector Machine [64] and Wavelet neural network [65] based equalizers [67].

Note that, in general, both the Bayesian TE and Bayesian DFE cannot achieve the theoretical best performance bound set by the adaptive sequence based MLVA since they are only symbol-decision equalizers. However, in a preliminary study [62], Chen et al. have shown that for highly non-stationary channels such as multi-path mobile radio fading channels, the adaptive Bayesian DFE is actually superior to the adaptive MLVA.

A classification of the various equalizers (some of which have been briefly reviewed in this chapter), in terms of types, structures and algorithms is given in Figure 5.2. This Chart extends that reported by Proakis [66] and Hussain [59].

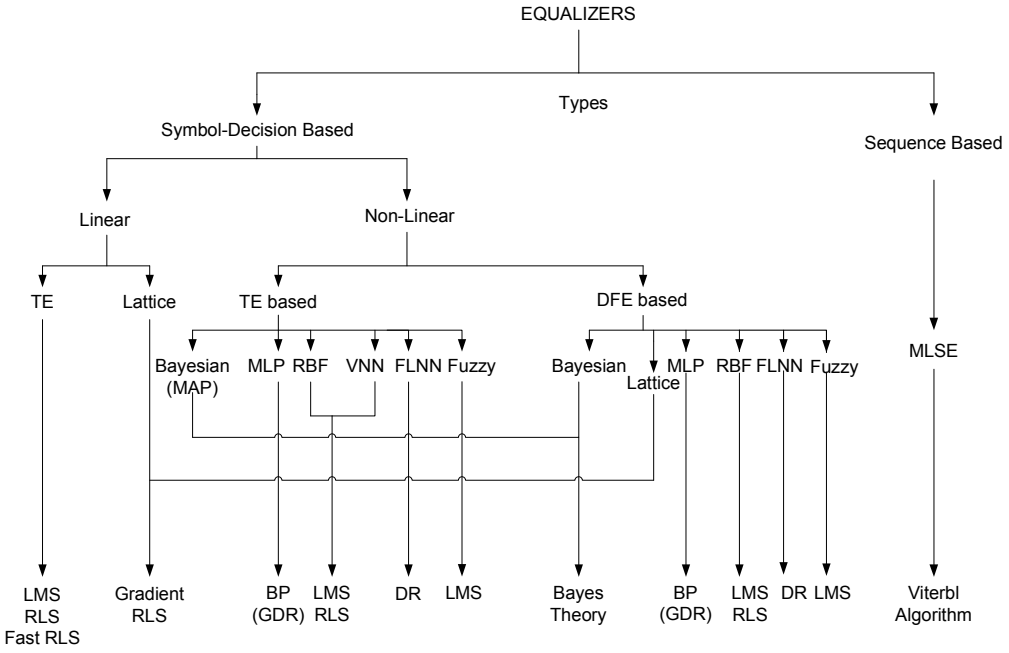

Figure 5.2: Classification of various equalizers types and algorithms

In the next section, the performance of selected neural network based equalizers is compared.

5.4 Simulation Results

First, in order to highlight the basic concepts involved in the equalization of the above co-channel system we first present an example by considering the following co-channel system:

$$H_0(z) = 1.0 + 0.5z^{-1} \qquad (5.8)$$

$$H_1(z) = \beta(1.0 + 0.2z^{-1}) \qquad (5.9)$$

Let SIR = 10dB which gives rise to $\beta = 0.346$. For the above co-channel system, use of 2 – *ary* PAM input signal and an equalizer of order m = 2 with delay $\tau = 0$, results in 8 desired signal states (that is, outputs from primary distorting channel H_0) and 8 interfering signal states (that is, outputs from the interfering co-channel H_1). The total number of channel observation states (that is, the overall outputs from the co-channel system $y(k)$) are thus 64 [48] which are plotted in the state diagram of figure 5.3, where the circles o's represent the desired channel states when a $s_0(k-\tau) = +1$ input symbol is transmitted, and the crosses x's represent the desired channel states for a -1 transmitted input. The dots in figure 5.3 represent noise free channel observation states (that is output from the co-channel system without the addition of Gaussian noise), the observations will form clusters with the means of these data clusters obviously being the noise-free observations, and their variance equal to that of the noise σ_n^2. As can be seen from figure 5.3, the composite effects of the distorting channel and the interfering co-channels has led to the noise free observations forming clusters around the desired signal states. It can be easily shown that for a high SIR value, the noise observations

states will concentrate around the desired signal states, whereas for a low SIR the nois-free observations states becomes more widely spread. In figure 5.3, the optimal decision boundary for this co-channel system [59], for the case of additive noise power of σ_n^2=0.0125 is also shown in a dotted line. The optimal decision boundary partitions the observation space (which is also the equalizer input space) into two decision regions. When an observation vector $(y(k),...,y(k-m+1)) = (y(k)y)k-1))$ appears in the right hand region of the boundary, the underlying optimal Bayesian decision function (which was derived for co-channel systems in [48] by Chen and Mulgrew) is positive and a decision $\hat{s}_0(k-\tau)=+1$ is made corresponding to a transmitted $s_0(k-\tau)=+1$. If an observation vector appears in the left hand region of the optimal boundary then a decision $\hat{s}_0(k-\tau)=-1$ is made (as the optimal Bayesian decision function is negative) corresponding to a transmitted $s_0(k-\tau)=-1$. This way of making symbol decisions (based on the values of the optimal Bayesian decision function) is optimal because it produces the minimum average error probability or BER [59]. Note that it can be clearly seen from Figure 5.3 that a non-linear equalizer will be required to approximate the optimal non-linear Bayesian decision boundary and the performance of linear equalizers (such as the LTE) would be sub-optimal as they are only capable of forming linear decision boundaries [48,59,68].

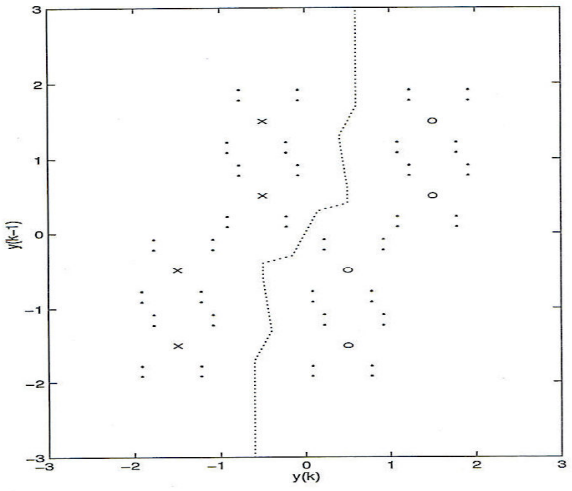

Figure 5.3: Outputs of Co-channel System for 2-ary PAM input and transmission delay = zero. The o and x denote desired signal states (+1 and -1 respectively), and the dots indicate the noise-free observation states. The dotted line is the approximate optimal Bayesian decision boundary.

Next, a second scenario was simulated as follows:

As in [53][67] a severe amplitude distorted co-channel involving one interfering co-channel, represented by $H_0(z) = 0.3482 + 0.8704z^{-1} + 0.3482\ z^{-2}$ and $H_1(z) = \lambda(0.6 + 0.8\ z^{-1})$, is used to compare the performance of the following equalizers (all of which were implemented in MATLAB):

i. The conventional Linear Transversal Equalizer (LTE) (additional details can be found in [48])

ii. The Radial Basis Function Neural Network based Transversal Equalizer (additional details in [48] [59])

iii. The newly reported Decision Feedback Wavelet Neural Network-Based Equalizer (DFWNE) (additional details can be found in [67])

iv. The Decision Feedback Functional Link Equalizer (DFFLE) (additional details in [53])

For a fair comparison, following [59] and [67], all the transversal equalizers employed above (LTE and RBF) were chosen to be of order 4 and the equalization delay was set to (τ = 1). The decision feedback equalizers were simulated with a feed forward and feedback order of 2 and 2, respectively, and an identical delay τ = 1. The training of all equalizers was stopped when the error had reached a steady state as in [67].

The best configurations for all the considered equalizers were determined beforehand using a trail and error basis (namely the hidden-layer size and choice of the transfer function for the Wavenet, the number of functional terms for the DFFLE and the number of centres and spreads for the RBF). These trial results were computed with a SNR = 15dB and a SIR = 15dB (which gives to a global SINR=12dB).

For the case of the wavelet based equalizer (DFWNE), following [55][67], a sigmoidal transfer function and a hidden layer size of 4 was experimentally selected, and an incremental gradient descent update rule was used to adapt the weights. For the case of the DFFLE, following [53], a number of 41 functional terms (comprising a combination of trigonometric and polynomial subset basis functions) were selected and the Delta Rule (DR) update was employed. For the case of the RBF, following [48,59], a total of 64 Gaussian basis functions with randomly selected centres (and spreads) were selected and the Least Mean Squares (LMS) weight update was employed. The LTE weights

(associated with the four equalizer input taps) were also adapted using the conventional LMS algorithm. The best step sizes for all the equalizers' weight update rules were determined experimentally and the training period for each equalizer was chosen to allow convergence to the lowest possible MSE on the training data set. The Bit Error Rate (BER) results on the test set were obtained from the averaging of ten independents runs over a hundred thousand bipolar test samples as in [48, 53, 67].

In order to evaluate the performance of the above equalizers, two scenarios where simulated as described below [53]:

Case 1: A value of $\lambda = 0.0631$ was chosen to provide a constant SIR = 24 dB, and the noise power was varied to produce different SINRs.

Case 2: The noise power was fixed to $\sigma_n^2 = 0.00398$ giving rise to constant SNR = 24 dB. Then, the interfering signal power was changed by choosing different values of λ.

The BER results are shown in figure 5.4 for case 1, and in figure 5.5 for the second case. As can be seen from Figures 5.4 and 5.5, the DFFLE gives the best BER performance, followed by the RBF, the DFWNA and the conventional LTE for both Cases.

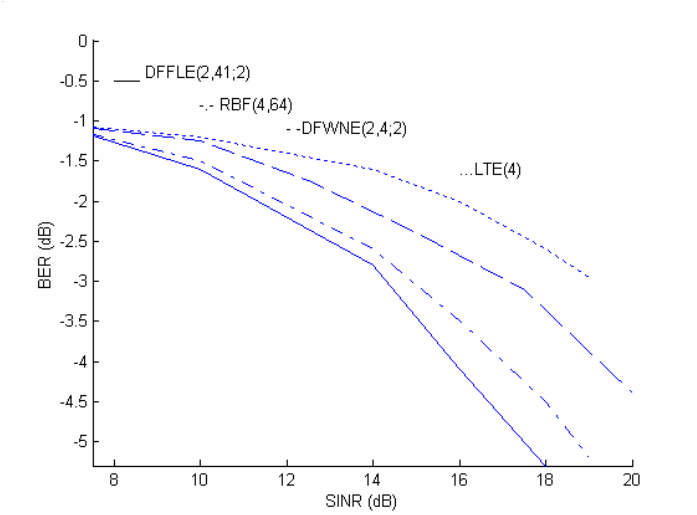

Figure 5.4: Case 1: BER Performance Comparison for SIR fixed at 24dB, and Noise Power σ_n^2 varied to produce different SINRs.

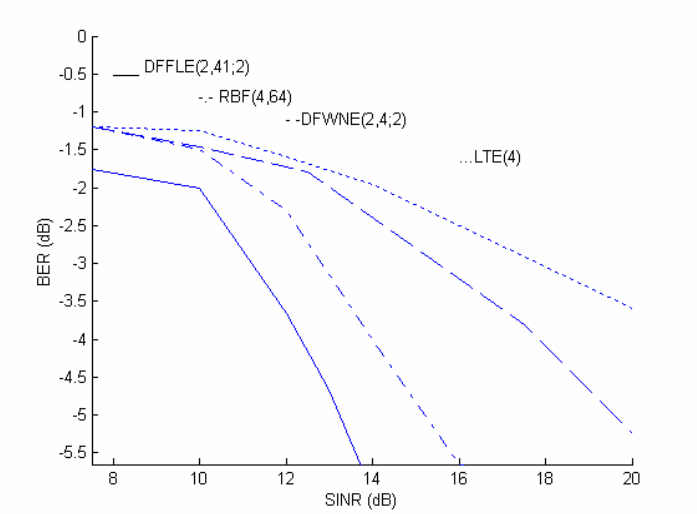

Figure 5.5: Case 2: BER Performance Comparison for SNR fixed at 24dB and λ varied to produce different SINRs.

5.5 Discussion and Conclusions

Comparing Figures 5.4 and 5.5 for the two Cases, it can be seen that the two BER curves of the linear LTE equalizer are similar confirming previous studies that it cannot distinguish between the interfering signal from the noise [48, 53, 59, 63, 70]. The best the LTE can do is to treat the interfering signals as additional coloured noise. This is due to its inability to form non-linear decision boundaries. On the other hand, the BER performance curves of all the non-linear equalizers (DFFLE, DFWNE and RBF) are seen to exhibit significant differences (particularly at high SINR values) with the performance obtained by changing the SIR for a fixed SNR (Case 2) being markedly better than that obtained by changing the SNR for a fixed SIR (Case 1), which is also consistent with previous studies [48,53,70], This confirms that the non-linear equalizers treat the noise and interference signals differently and are more effective in approximating the optimal equalizer solution on account of their inherent non-linear decision making capability. As can be seen from Figures 5.4 and 5.5, the DFFLE gives the best overall BER performance at all SINR values for both Cases, followed by the RBF and the DFWNE. The LTE provides the worst performance as expected on account of its inability to form the required non-linear classification/decision boundaries..

It was shown in [48] that computing the optimal Bayesian transversal equalizer for the above co-channel system is extremely costly. The full RBF network able to realize the optimal solution would need a total of 2048 centres corresponding to the number of

observation states = number of desired states (64) x number of interfering states (32)) which makes the calculation of BERs impractical. Hence the DFFLE based structure requiring just 41 functional terms (or basis functions), is a viable alternative to the (4,64) RBF, the (2,4;2) DFWNE, and the (4)LTE structures for providing a close approximation to the underlying optimal co-channel equalization solution.

To conclude, this chapter has reviewed the problem of adaptive equalization of digital communication channels in the presence of ISI, AWGN and co-channel interference. A realistic co-channel system was used as a case study to demonstrate the equalization capability of selected neural network based equalizers. The results have shown better BER performance characteristics for the functional-link-DFE, compared to the conventional LTE, DFE, wavenet and RBF equalizers. Note that the parameters of all the neural network equalizers were all determined experimentally using a trial and error approach and are thought to be reasonable but these could be further optimised. The results in this study have considered single co-channel systems, but they can be readily extended to the multi-co-channel case.

For future work, the error propagation properties of the functional-link DFE and the wavenet DFE need investigation (due to the possible feedback of incorrect detected bits affecting future decisions [59][65][67]), and a more detailed theoretical analysis is required to define their attainable performance. The performance of the proposed equalizers also needs to be compared with the optimal Bayesian DFE and MLVA based approaches (both of which require a priori knowledge of the channel and interfering co-

channel orders for combating the co-channel interference problem in mobile cellular networks [53, 67, 68]

Chapter 6

6 Conclusions and Future Work Directions

6.1 Conclusions:

This thesis has presented new neural network based approaches for tackling two important problems encountered in cellular networks, namely prediction of mobile locations and co-channel interference suppression.

An overview of radio wave principles and various propagation models reported to-date was first presented in Chapter 2. Next, the predominant location estimation techniques in use were critically evaluated in Chapter 3. Next, Chapter 4 presented an overview of a few selected conventional neural network paradigms, including the most widely used feedforward Multi Layer Perceptron (MLP), and the Radial Basis Function (RBF) based Generalized Regression Neural Network (GRNN), and then described their novel use for location estimation in cellular networks. The application of neural networks discussed in this thesis was considered as a function approximation problem consisting of a non-linear mapping of signal strength input (received at several Base Stations) onto a dual output variable representing the mobile location co-ordinates.

Simulation results were presented assessing the generalization performance of neural network based location predictors and compared with a linear adaptive filtering based

approach. The simulated signal strength data was first generated using a COST 231-Walfisch Ikegami Non-line of Sight (NLOS) model on account of its extensive use in practice in typical suburban and urban environments where the building heights are quasi-uniform. The designers of the public mobile radio systems (e.g., GSM, PCS, DECT, DCS, etc.) also often use this model [10]. The MDE performance of the various location predictors was compared on the COST-231 model and the MLP location predictor was found to be more effective than the RBF based GRNN and linear predictors. Preliminary findings using very limited real data were also presented and discussed which showed that the neural predictors are capable of providing highly accurate location estimates even in the case of very limited real data from just two BSs. This is an interesting finding which needs further investigation (using more extensive real data from a range of urban and indoor environments).

Next, Chapter 5 presented an overview of the co-channel interference problem in cellular networks, including the conventional approaches that have been developed to-date. Following the overview, selected neural network based equalizers were employed for co-channel interference suppression using a realistic co-channel system. Simulation results demonstrated superior Bit Error Rate (BER) performance for the Functional-Link neural network based DFE compared to other conventional linear and non-linear equalizers, particularly at low SINR values. The overview of adaptive equalizers presented in this chapter has shown the need for developing new efficient non-linear equalizers that can effectively approximate the optimal Bayesian DFE with comparatively reduced computational requirement.

6.2 Future Work Directions

Many issues and research topics related to this research thesis were not addressed and accomplished in this thesis due to limitations in time and resources. In this section, some of these issues are suggested and outlined for possible future study.

- The performance of the neural network based location estimators needs to be further evaluated using extensive real data for a range of environments. Their performance also needs to be compared with other neural network and non-linear function approximation techniques not considered in this thesis.
- Note that in this study, different grid sizes were used to generate the simulated training and test sets. However, other more conventional ways could also be explored, such as, by randomly dividing parts of the same data (generated at a fixed grid size) for both training and test purposes. An approach similar to this was adopted for the case of very limited real signal strength data used in section 4.4.2. Comparison of the various approaches reported in literature [38] for selection of training and test sets needs to be carried out and their effect on the performance of the neural network location predictors evaluated.
- The performance of neural network location predictors needs to be compared (in terms of performance-complexity trade-off) with several other techniques that are currently available for determining mobile location, based on a variety of measuring schemes, which include time of arrival (TOA), time difference of arrival (TDOA), angle of arrival (AOA) and assisted GPS (A-GPS) [6].

- Detailed theoretical analysis of attainable performance and detailed practical (hardware and software) implementation aspects also need to be considered for the proposed neural network based mobile location predictors for further work.
- The possibility of using neural network location predictors in conjunction with other recently reported statistical location estimation techniques [52] can also be explored, in order to further improve their performance.
- The preliminary work reported in this thesis on location estimation of mobile users can be extended to deal with the more challenging case of locating moving vehicles etc. [52] in which case the signal strength and the mobile station velocity could be used together to provide accurate location predictions through the use of neural networks. This would be an interesting and challenging topic for future research.
- Future work is also required to develop interference models that can be used to predict levels of co-channel interference and identify sources of interference in digital communications systems. The developed models will need to cover system-specific interference modelling to determine CCI from both immediate and adjacent cells. Whilst, several standard propagation models are accepted by industry [10] (i.e. Okumura and COST-231/Walfish/Ikegami as discussed in this thesis), no interference models have been developed or accepted to-date according to our knowledge. This area of research is currently being investigated by the Institute for Telecommunication Sciences (ITS) who are aiming to develop a series of Personal Communication Services (PCS) interference models that cover 3G systems [69, 74].

- For future work, a detailed theoretical analysis of the neural network based equalizers is required to define their attainable performance. The performance of the neural network equalizers evaluated in this thesis also needs to be compared with other emerging neural network and soft computing based approaches, including the Support Vector Machine [64] [67], Fuzzy [63] [70], Recurrent Neural Networks [71] as well as with optimal Bayesian DFE and MLVA based approaches [68] for combating the co-channel interference problem in mobile cellular networks.
- Another interesting possibility, following the recent work of [56], could be to investigate the possible use of neural network based DFEs for developing an alternative model for expected throughput in a Bluetooth network in the presence of a number of other Bluetooth networks that cause radio interference. The results from this work could prove potentially useful when designing ad-hoc networking functionality for future versions of Bluetooth.
- Also in chapter 5, single co-channel systems have been considered and therefore, the multi co-channel interference scenario can be readily simulated. It is also important to note that all results presented in chapter 5 were for 2-ary baseband PAM systems, and therefore extensions of the reported equalizer structures to multi-level M-ary PAM and QAM based systems need to be investigated and compared with the existing techniques [57]. One way to equalize M-ary PAM signals would be to employ multi-output equalizers (similar to the multi-output RBF equalizer reported by Chen and Grant et al [58]) with one output node assigned to each class. However with this approach

the equalizer complexity will increase in proportion with the number of transmitted symbol categories. Alternatively, a single multi-level sigmoidal function can be employed, for example, in the wavelet and functional-link DFE equalizers' output layer as follows [47]:

$$\hat{s}_0(k-\tau) = \sum_{j=-((M/2-1))}^{(M/2-1)} \frac{1-e^{(-\alpha o_k + hj)}}{1+e^{(-\alpha o_k + hj)}} \qquad (6.1)$$

Where o_k is the output from the linear combiner, and the constants α and h are referred to as the slope and drift parameters respectively, which have been shown in [47] to give efficient equalization performance with values set to ($\beta = 1.0$) and ($h = 15$). The functional-link and wavelet basis functions used within their single hidden layers would also need to be modified to accommodate M-ary PAM signalling. This would simply involve scaling all the basis functions by a scaling factor A, which for M-ary PAM will be A=(M-1). This scaling factor will enable the basis functions to cover the new range (-(M-1),(M-1)), from their previous (-1,+1) range employed for 2-ary PAM signalling.

- Also for future work, application of the neural network based equalizers to Code Division Multiple Access (CDMA) Spread Spectrum (SS) communication systems can be investigated, and their performance compared (in terms of performance-complexity trade-off) with the optimal Bayesian DFE methods which have been successfully applied to CDMA systems [68].
- The use of the neural network equalizer structures in blind adaptive equalization schemes can also be investigated. This may also include these equalizers operating in hybrid systems, where for example, a computationally expensive Higher Order

Statistics (HOS) based blind equalizer initially estimates the channel coefficients, and the system then switches to the computationally efficient functional-link DFE or other neural network based adaptive non-linear equalizers operating in Decision Direct Mode (DDM), as in [61]. Finally, application of the functional-link and wavenet DFE structures to equalization of non-stationary communication channels such as those encountered in fading mobile radio environments [68]) also needs to be investigated.

- Note that since the performance of a communication system is often evaluated in terms of BER, intuition suggests that the equalizer is optimised when the probability of error is minimised. However the probability of error is a highly non-linear function of the equalizer tap coefficients [66], and the solution to this problem is mathematically intractable. Finding an analytical solution or its approximation is a challenging yet interesting future research topic. Furthermore, the convergence of the various equalizers (in terms of the average mean squared error) was not compared in this thesis, and finding and comparing the average MSE is also a good topic for theoretical analysis.
- Lastly, it should be noted that whilst this thesis has presented the application of neural networks to two important problems encountered in cellular networks, namely prediction of mobile locations and co-channel interference suppression, there are there are many links and similarities between the two problems considered, and the techniques used, but the second problem investigation has used little knowledge and experience gained from the first investigation. This is proposed for future work.

References

[1] Wamiq M.Ahmed, Amir Hussain & Syed I. Shah, "Location Estimation in Cellular Networks using neural networks", Proc. International (NAISO-IEEE) Symposium on Info. Science Inovations (ISI'2001), Dubai, 19-21 March 2001

[2] B.E. Gschwendtner and F.M. Landstorfer, "Adaptive propagation modelling using a Hybrid Neural Technique", Electronics Letters, vol. 32, pp. 162-164, Feb.1996

[3] P-R. Chang, W-H Yang, "Environment-Adaptation Mobile Radio Propagation Prediction Using Radial basis Function Neural Networks", IEEE Trans. Vech. Technology , vol. 46, no, 1, pp 155-160, Feb.1997

[4] Wayne M.Saslow, 2002, Electricity, Magnetism, and Light, Academic Press, ISBN-13:978-0126194555

[5] NAWC, Naval Air Warfare Center. 1997 (Apr.). "Electronic warfare and Radar Systems EngineeringHandbook",Tech. rept. TP 8347. www.ewhdbks.mugu.navy.mil

[6] Theodore S. Rappaport, 2002, Wireless Communications: Principles and Practice, Prentice Hall PTR, ISBN: 9780130422323.

[7] Walke B. 2004, Mobile Radio Networks: Networking, Protocols and Traffic Performance, ISBN-13:978-0470846247

[8] Xu,H., Rappaport, T.S., Boyle, R.J., & Schaffner, J.H. 2000, "Measurements and Models for 38-GHz Point-to-Multipoint Radiowave Propagation". IEEE Journal on Selected Areas in Communications, 18(3), 310_321.

[9] F.D.Cardoso, S.Taccori, L.M.Correia, IST-2001-32125 FLOWS, Initial Propagation Models. pp.20, 2002

[10] Aleksandar Neskovic, Natasa Neskovic, and George Paunovic, "Modern Approaches in Modelling of Mobile Radio Systems Propagation Environment", IEEE Communications Surveys, http://www.comsoc.org/pubs/surveys, 2002

[11] CCIR Study Groups Period 1978–1982, European Broadcasting Union, "Improvement of Predictions of Field Strengths in VHF and UHF Bands," Doc. 5/28-E, 1980.

[12] A. G. Longley and P. L. Rice, "Prediction of Tropospheric Radio Transmission Loss Over Irregular Terrain, A Computer Method, 1968," Inst., Telecommun. Sci., ESSA Tech. Rep ERL79-ITS67, Boulder, Co.

[13] Lee, Mobile Communications Design Fundamentals, 2nd Ed. John Wiley & Sons Inc., ISBN: 978-0471007470, 1994

[14] IEEE Vehic. Tec. Society, Special Issue on Mobile Radio Prop., IEEE Trans. Vehic. Tech., vol. 37, 1988, pp. 3–72.

[15] C. Dadson, J. Durkin, and R. Martin, "Computer Prediction of Field Strength in the Planning of Radio Systems," IEEE Trans. Vehic. Tech., vol. 24, no. 1, 1975.

[16] "EET-Ericsson Engineering Tool, User Reference Guide," Ericsson Radio Systems AB, 1997.

[17] K. Bullington, "Radio Propagation for Vehicular Communications," IEEE Trans.Vehic. Tech., vol. VT–26, no. 4, Nov. 1977, pp. 295–308.

[18] A. Neskovic, N. Neskovic, and D. Paunovic, "A Field Strength Prediction Model Based on Artificial Neural Networks," Proc. 9th IEEE Med. Electro. Conf. – MELECON, Tel Aviv – Israel, May 1998

[19] S. Y. Tan and H. S. Tan, "A Microcellular Communications Propagation Model Based on the Uniform Theory of Diffraction and Multiple Image Theory," IEEE Trans. Ant. and Prop., vol. 44, no. 10, Oct. 1996

[20] K. Pahlavan and A. H. Levesque, Wireless Information Networks, Wiley, ISBN: 978-0471725428, 2005.

[21] Y. Okumura et al., "Field Strength and its Variability in VHF and UHF Land-Mobile Services," Review Elec. Commun. Labs., vol. 16, Sept.–Oct., 1968, pp. 825–37.

[22] K. Allsebrook and J. D. Parsons, "Mobile Radio Propagation in British Cities at Frequencies in the VHF and UHF Bands," IEEE Trans. Vehic. Tech., vol. VT-26, no. 4, Nov. 1977, pp. 313–23.

[23] D. Paunovic, Z. Stojanovic, and I. Stojanovic, "Choice of a Suitable Method for the Prediction of the Field Strength in Planning Land Mobile Radio Systems," IEEE Trans. Vehic. Tech.,vol. 33, no. 3, 1984, pp. 259–65.

[24] M. Hata, "Empirical Formula for Propagation Loss in Land Mobile Radio Services," IEEE Trans. Vehic. Tech., vol. 29, no. 3, 1980.

[25] A. Mehrotra, Cellular Radio Performance Engineering, Artech House, 1994.

[26] J.S. Lee and L.E. Miller, CDMA systems Engineering Handbook, Boston: ArtechHouse, 1998.

[27] Fleury, B.H., and P.E. Leuthold, “Radiowave Propagation in Mobile Communications: An Overview of European Research,” IEEE Communications Magazine, pp. 70-81, Feb.1996.

[28] Stuber, G. L., Principles of Mobile Communication, Springer, ISBN: 978-0792379980, 2000

[29] “Propagation Prediction Models,” COST231 Final Rep., ch.4, pp. 17-21.

[30] H. H. Xia et al., “Radio Propagation Characteristics for Lineof-Sight Microcellular and Personal Communication,” IEEE Trans. Ant. and Prop., vol. 41, no. 10, Oct. 1993.

[31] R. J. Luebbers, “Finite Conductivity Uniform GTD Versus Knife-edge Diffraction in Prediction of Propagation Path Loss,” IEEE Trans. Ant. Prop., vol. AP-32, Jan. 1984, pp. 70–72.

[32] R. G. Kouyoumijan and P. H. Pathak, “A Uniform Theory of Diffraction for an Edge in a Perfectly Conducting Surface,” Proc. IEEE, vol. 62, Nov. 1974, pp. 1448–61.

[33] K. Pahlavan and A. H. Levesque, Wireless Information Networks, New York: John Wiley & Sons, Inc., 1995.

[34] Vipul Sawhney, “Location Based Services,” Columbia University

[35] S. C. Agarwal & S. Agarwal, “Location Based Services,” September 2003, TATA Consultancy Services

[36] K.Raja, WJ. Buchanan and J. Munoz, “Location Tracking,” The IEE Communications Engineer, pp.34-39, June/July 2004.

[37] J. Muhammad, A. Hussain, Alexander Neskovic & Evan Magill, "New Neural Network Based Mobile Location Estimation in a Metropolitan Area", Lecture Notes in Computer Science, Springer Berlin / Heidelberg, ISSN: 0302-9743, Volume 3697/2005, pages 935-941, Artificial Neural Networks: Formal Models and Their Applications - ICANN 2005 , ISBN: 978-3-540-28755-1

[38] Haykin, S, Neural Networks: A Comprehensive foundation, 2nd Edition, Prentice Hall, 1998, ISBN: 978-0132733502.

[39] http://electronics.howstuffworks.com/gps1.htm

[40] Specht, D.F., 1991, "A General Regression Neural Network", IEEE Tras. Neural Networks, 2(6), 568-576

[41] P.D. Wasserman, 1993, "Advanced Methods in Neural Computing", New York, Van Nostrand Reinhold, pp. 155-61

[42] The Electronic Journal of Geotechnical engineering, Vol. 4, 1999, “Artificial Intelligence Techniques for the Design and Analysis of Deep Foundations”, N.O.Nawari, R.Liang, and J.Nusairat, university of Akron, Akron, OH, USA.

[43] S.Chen, G,J.Gibson, C.F.Cowan, P.M.Grant, Adaptive equalization of finite non-linear channels using Multi-Layered Perceptrons, Signal Processing, pp.107-119, 1990.

[44] N.Beamish, A.D.Fagan, On the equalization of baseband LNL channel, EUSIPCO Proc., pp.1528-1531, Edinburgh, U.K., September 1994.

[45] G.J.Gibson, S.Siu, C.F.N.Cowan, Multilayer Perceptron Structures Applied to Adaptive Equalizers for Data Communications, IEEE ICASSP, pp1183-1184, Glasgow 1989.

[46] S.Chen, G.J.Gibson, C.F.Cowan, Adaptive Channel Equalization using a polynomial-perceptron structure, IEE Proc., vol.137, pt.I, no.5, pp257-264, 1990

[47] K.Hacioglu, M.Abdelhafez, Reconstruction of PAM signals using a multi-layered perceptron with a multi-level sigmoidal function, EUSIPCO proc., pp.1811-1514, Edinburgh, U.K., September 1994

[48] S.Chen, B.Mulgrew, Overcoming co-channel interference using an adaptive radial basis function equalizer, Signal Processing 28, Elsevier, pp 91-107, 1992

[49] J.C.Campbell, A.J.Gibbs, B.M.Smith, The cyclostationary nature of crosstalk interference from digital signals in multipair cable – Part I: fundamentals; Part II: applications and further results, IEEE Trans. Comm., Vol.COM-31, no.5, pp,629-649,1983.

[50] K.Giridhar, S.Chari, J.J.Shynk, R.P.Gooch Joint demodulation of co-channel signals using MLSE & MAPSD Algorithms, IEEE ICASSP, Vol.4, pp.160-163, 1993.

[51] Location-based Services, Geo Informatics, April; 2001, www.geoinformatics.com

[52] M. Aso, T. Saikawa, T. Hattori, Maximum Likelihood Location Estimation using Signal Strength and the Mobile Station Velocity in Cellular Systems, Proc. IEEE Vehicular Technology Conference, 2003

[53] A. Hussain, T.S.Durrani, “A New Adaptive Functional-link Neural Network based DFE for overcoming co-channel interference”, IEEE Trans. Communications, 45(11), 1997

[54] G.J.M.Janssen, BER and outage performance of a dual signal receiver for narrowband BPSK modulated co-channels in a Rican fading channel, Personal and Indoor mobile radio Conference, The Hague, pp.601-606, 1994.

[55] Y. Oussar, I. Rivals, L. Personnaz, G. Dreyfus "Training Wavelet Networks for Nonlinear Dynamic Input-Output Modelling", Neurocomputing, Elsevier, 1998

[56] Simon Baatz, Matthias Frank, Peter Martini, Christoph Scholz, "A Worst-Case Model for Co-Channel Interference in the Bluetooth Wireless System," lcn, p. 346, 28th Annual IEEE International Conference on Local Computer Networks (LCN'03), 2003.

[57] S.Chen, B.Mulgrew, P.M.Grant, Clustering techniques for Digital Communications Channel Equalization Using RBF Networks, IEEE Trans. On Neural Networks, Vol.4, July 1993.

[58] S.Chen, P.M.Grant, C.F.N.cowan, Orthogonal Least Squares Algorithm for Training Multi-Output Radial basis Function Networks, proc., IEE 2nd Intern.confer. on Artificial Neural Networks, pp.336-339, Bournemouth Intern. Centre, U.K., November, 1991.

[59] A.Hussain, Novel Artificial Neural Network Architecture and Algorithms for non-Linear Dynamical Systems modelling and Digital communications Applications, PhD Thesis, 1996.

[60] S. W. Wales, Technique for co-channel interference in TDMA mobile radio systems, IEE Proceedings – Communications, 142(2), 106-114, 1995.

[61] A. Alkulaibi, J. Soraghan, A. Hussain, Hybrid higher order cepstrum and functional-link network (HOCFLN) based blind equalizer, Proc. IEEE DSP Workshop, 446-449, 1-4 Sep 1996.

[62] Chen, S. McLaughlin, S. Mulgrew, B. Grant, P.M., Bayesian decision feedback equaliser for overcoming co-channel interference, IEE Proceedings, Aug 1996, Vol: 143, Issue: 4, pp: 219-225

[63] Patra, S.K. Mulgrew, B., Fuzzy implementation of a Bayesian equaliser in the presence of inter-symbol and co-channel interference Communications, IEE Proceedings, Oct 1998, Vol: 145, Issue: 5, pp: 323-330

[64] S. Chen, S. Gunn, C.J. Harris, Decision Feedback Equalizer Design using SVM, IEE Proceedings, Vision, Image & Signal Processing 147(3), 213-219, 2000

[65] Feng Liu Jun Cheng Jinbiao Xu Xinmei Wang, Wavelet based adaptive equalization algorithm, Global Telecommunications Conference, 1997. GLOBECOM '97., IEEE Publication, 3-8 Nov 1997, Vol: 3, pp: 1230-1234.

[66] J.G. Proakis, Digital Communications, McGraw-Hill, New York, 1995

[67] A. Olivier, A. Hussain, "Computational Intelligence Techniques for overcoming co-channel interference in mobile cellular networks", IEE/IEEE International Workshop on Signal Processing for Wireless Communications (SPWC'2003), King's College, London.

[68] Sheng Chen McLaughlin, S. Mulgrew, B. Grant, P.M., Adaptive Bayesian decision feedback equalizer for dispersive mobileradio channels, IEEE Transactions on Communications, May 1995, Vol: 43, Issue: 5, pp: 1937-1946

[69] http://glossary.its.bldrdoc.gov/programs/its_e/pcs/PCS_Interference_Modeling

[70] Patra S.K, Mulgrew B., Fuzzy techniques for adaptive non-linear equalization, Signal Processing, Vol: 80, Number 6, June 2000, pp. 985-1000(16)

[71] Jongsoo Choi Lima, A.Cd.C. Haykin, S, Kalman filter-trained recurrent neural equalizers for time-varying channels, IEEE Transactions on Communications, March 2005, Vol.53, Issue 3, pp. 472-480.

[72] H. Sizun, P.de Fornel, 2004, Radio Wave Propagation for Telecommunication Applications, Springer, ISBN: 978-3540407584

[73] Kyoung Il Kim, 2000, Handbook of CDMA System Design, Engineering and Optimisation, Prentice Hall PTR, ISBN-13: 978-0130175724

[74] H.H.Chen, 2007, The Next Generation CDMA Technologies, John Wiley and Sons Ltd, ISBN: 978-0470022948

[75] Ostlin, E. Zepernick, H.-J. Suzuki, H., 2004, Macrocell radio wave propagation prediction using an artificial neural network, IEEE 60th , Vehicular Technology Conference, 2004. VTC2004-Fall. 2004, Volume: 1, Page(s): 57- 61 Vol.1, ISSN: 1090-3038, ISBN: 0-7803-8521-7